Chapter 3

Fabrication of Bragg Gratings

3.1 Methods for fiber Bragg grating fabrication

This chapter reviews many of the schemes proposed for both holographic and nonholographic grating inscription and considers some of the salient features of the methods. This introduction excludes methods used for internal grating writing, traditionally known as "Hill" gratings, for which the reader is directed to other sources [1–12].

Fiber Bragg gratings, which operate at wavelengths other than near the writing wavelength (non-Hill gratings), are fabricated by techniques that broadly fall into two categories: those that are holographic [13] and those that are noninterferometric, based on simple exposure to UV radiation periodically along a piece of fiber [14]. The former techniques use a beam splitter to divide a single input UV beam into two, interfering them at the fiber; the latter depend on periodic exposure of a fiber to pulsed sources or through a spatially periodic amplitude mask. There are several laser sources that can be used, depending on the type of fiber used for the grating, the type of grating, or the intended application. The sources used for grating production are also discussed in this chapter.

3.1.1 The bulk interferometer

The method for the side writing of fiber gratings demonstrated by Meltz *et al.* [15] is shown in Fig. 3.1. The interferometer is one encountered in

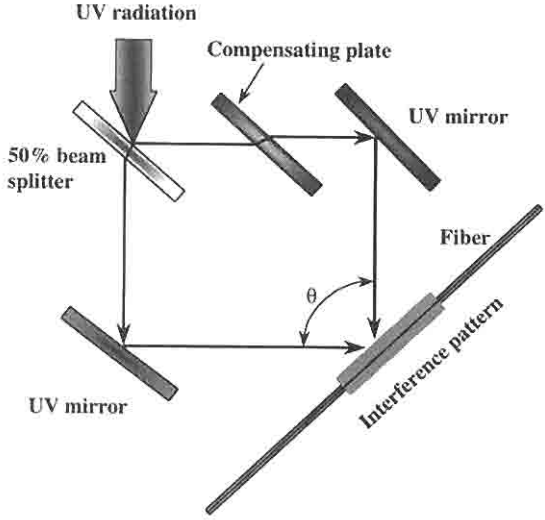

Figure 3.1: UV interferometer for writing Bragg gratings in optical fibers. Note the use of an additional phase plate (mirror blank) in one arm to compensate for the path length difference.

standard holography [16], with the UV beam divided into two at a beam splitter and then brought together at a mutual angle of θ, by reflections from two UV mirrors. This method allows the Bragg wavelength to be chosen independently of the UV wavelength as

$$\lambda_{Bragg} = \frac{n_{eff}\lambda_{uv}}{n_{uv}\sin\left(\frac{\theta}{2}\right)}, \tag{3.1.1}$$

where λ_{Bragg} is the Bragg reflection wavelength, n_{eff} is the effective mode index in the fiber, n_{uv} is the refractive index of silica in the UV, λ_{uv} is the wavelength of the writing radiation, and θ is the mutual angle of the UV beams. The essential difference between a "Hill" grating and one produced by external interference of two UV beams is that with the holographic technique the Bragg reflection wavelength depends on UV radiation wavelength and geometric factors. Since λ_{uv} is around 240 nm, θ lies between 0° and 180°, and assuming that the refractive index in the UV is approximately equal to the effective index, the Bragg wavelength is adjustable from one nearly equal to the UV source wavelength to infinity [see Eq. (3.1.1) with $\theta = 0$].

The fiber is held at the intersection of the beams. This method was originally successfully used to write gratings at visible wavelengths. The interferometer is ideal for single-pulse writing of short gratings, and great care has to be taken in the design of the optical mounts. Mechanical vibrations and the inherently long path lengths in air can cause the quality of the interferogram to change over a period of time, limiting its application to short exposures. For low-coherence sources, the path difference between the two interfering beams must be equalized; a simple method is to introduce a mirror blank in one arm to compensate for the path imbalance imposed by the beam splitter, as shown in Fig. 3.1. Note that the in arriving at the fiber, the beam that is transmitted through the beam splitter undergoes a 180° rotation so that they have *different* spatial profiles. This is an important factor for spatially incoherent beams.

The interferometer shown in Fig. 3.1 has several beams paths in open air. It is important that these are shielded from turbulence, since the interference fringes formed at the fiber can drift if the paths of the two beams change during the inscription time. As is common with all holographic arrangements, it is not sensible to mount mirrors, beam splitters, or the fiber on flimsy platforms prone to disturbance, such as tall 10-mm diameter mounting posts. The interferometer needs to be built on a sturdy base, with stable optical mounts. This is especially true in cases that require long (minutes to hours) exposures. It is common practice to enclose the entire interferometer within a Perspex housing, which allows visual and physical access to the setup, at the same time protecting the interferometer from constant path-length variations and the operator from accidental exposure to UV radiation. Extreme care needs to be taken to minimize exposure of personnel to high-energy UV radiation or long-term exposure to low-power radiation. Adhering to safe operating practices is essential when using UV radiation.

In principle, a diffraction grating used in reflection can replace the 50% beam splitter shown in Fig. 3.1. In this interferometer, two coherent beams are required, so that reflection from a diffraction grating to divide the input UV beam into two is equally feasible. However, a simpler component, the transmission phase-grating, otherwise known as the *phase mask,* is better suited to this application.

3.1.2 The phase mask

A major step toward easier inscription of fiber gratings was made possible by the application of the phase mask as a component of the interferometer.

Used in transmission, a phase mask is a relief grating etched in a silica plate. The significant features of the phase mask are the grooves etched into a UV-transmitting silica mask plate, with a carefully controlled mark–space ratio as well as etch depth. The principle of operation is based on the diffraction of an incident UV beam into several orders, $m = 0, \pm 1, \pm 2 \ldots$. This is shown schematically in Fig. 3.2. The incident and diffracted orders satisfy the general diffraction equation, with the period Λ_{pm} of the phase-mask,

$$\Lambda_{pm} = \frac{m\lambda_{uv}}{\left(\sin\frac{\theta_m}{2} - \sin\theta_i\right)}, \tag{3.1.2}$$

where $\theta_m/2$ is the angle of the diffracted order, λ_{uv} the wavelength, and θ_i the angle of the incident UV beam. In instances when the period of the grating lies between λ_{uv} and $\lambda_{uv}/2$, the incident wave is diffracted into only a single order ($m = -1$) with the rest of the power remaining in the transmitted wave ($m = 0$).

With the UV radiation at normal incidence, $\theta_i = 0$, the diffracted radiation is split into $m = 0$ and ± 1 orders, as shown in Fig. 3.3. The interference pattern at the fiber of two such beams of orders ± 1 brought together by parallel mirrors (as in Fig. 3.1) has a period Λ_g related to the diffraction angle $\theta_m/2$ by

$$\Lambda_g = \frac{\lambda_{uv}}{2\sin(\theta_m/2)} = \frac{\Lambda_{pm}}{2}. \tag{3.1.3}$$

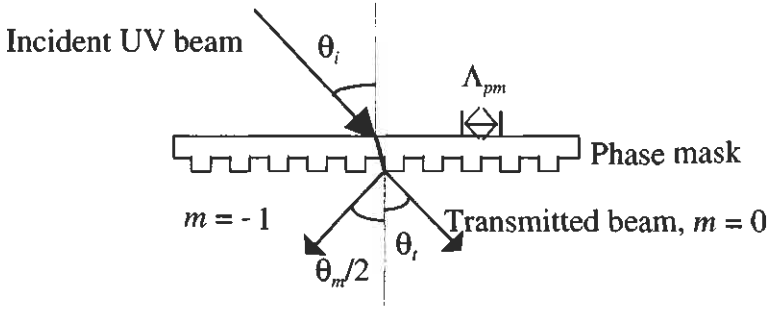

Figure 3.2: A schematic of the diffraction of an incident beam from a phase mask.

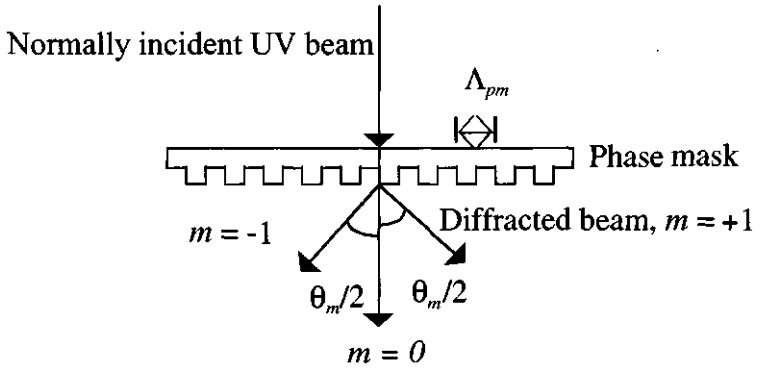

Figure 3.3: Normally incident UV beam diffracted into two ±1 orders. The remnant radiation exits the phase-mask in the zero order ($m = 0$).

The period Λ_{pm} of the grating etched in the mask is determined by the Bragg wavelength λ_{Bragg} required for the grating in the fiber (see Chapter 4) and using Eq. (3.1.3) to arrive at

$$\Lambda_g = \frac{N\lambda_{Bragg}}{2n_{eff}} = \frac{\Lambda_{pm}}{2}, \tag{3.1.4}$$

where $N \geq 1$ is an integer indicating the order of the grating period.

For *nonnormal* incidence of the UV radiation on the phase mask, intensities in the $m = 0$ and -1 orders are not necessarily equal. However, for the visibility of the interference pattern to be a maximum, the intensities must be equalized. This is important if gratings are to be inscribed efficiently. For a first-order ($N = 1$) grating at a Bragg wavelength of 1.55 μm and a mode effective index $n_{eff} \approx 1.46$, $\Lambda_{pm} = 1.06$ μm, which is greater than the wavelength of the UV radiation used for grating inscription (0.193 to 0.360 μm). Therefore, more than a single diffracted order ($m = 0, \pm 1, \pm 2 \ldots$) exists. To suppress the positive orders and control the diffraction efficiency, and to equalize the power between the -1 order and the transmitted beam ($m = 0$), one face of the etched grating walls may be coated with a metal film to form reflecting mirrors. This may be done by evaporating the metal on to the phase-mask plate at an angle so that only the walls facing the evaporation source are coated [17]. Another method uses a deeper etched grating in the phase mask [18] to suppress higher orders and control the relative intensities. However, it is easier

and more cost-effective simply to use a phase mask at normal incidence. If necessary, an antireflection coating may be applied to the back facet of the phase-mask plate to reduce reflections, which can cause the quality of the interference fringes to be degraded [25].

The depth d of the etched sections of the grating is a function of the UV wavelength, but the period is dependent only on the Bragg wavelength and the effective index of the mode. However, in the case of UV writing of gratings, it is necessary to ensure that the intensity of the transmitted zero-order beam is minimized and, ideally, blocked from arriving at the fiber.

To minimize the zeroth order from a UV beam normally incident on a phase mask, the smallest etch depth d of the relief grating in silica is,

$$d(n_{uv} - 1) = \lambda_{uv}/2. \tag{3.1.5}$$

Equation (3.1.5) assumes monochromatic radiation with no divergence; however, for a practical nonmonochromatic source, the $m = 0$ order cannot be eliminated. In practice, the zeroth order can be reduced to a level of a percent or so. At a wavelength of 244 nm, $d \approx 262$ nm. The phase-mask zero order can be nulled only at a single wavelength. Changing the laser source wavelength will require a different phase mask, unless the zero order is physically blocked. For efficient diffraction onto the first orders, it is necessary for the relief grating to have a mark–space ratio of 1:1, or for the corrugations in the phase mask to be purely sinusoidal.

Fabrication of the phase mask

The phase mask is normally fabricated by one of two methods: by exposure of a photoresist overcoated, silica maskplate to an electron beam to form the pattern [19,20], or by holographic exposure [21]. With the e-beam facility, a silica wafer, which has a bilevel resist comprising a 450-nm layer of AZI400-27 is hard baked at 190°C for 30 minutes, followed by a 200-nm layer of silicon-containing negative resist (SNR) baked at 85°C, also for 30 minutes. Charge dispersal during the e-beam exposure is effected by a evaporating a thin layer of aluminum. After exposure to delineate the pattern, the A1 coating is removed in an alkaline solution and the SNR spray developed in MIBK for 35 sec, then rinsed in a 50:50 ratio of MIBK+IPA solution for 5 sec, followed by 15 sec in IPA. The developed pattern is transferred to the AZI400-27 layer by reactive ion etching (RIE) at 10 m torr in oxygen and 50 W RIE. The resist is then

used as a mask for etching into the silica plate using CHF_3:Ar RIE. The final depth of 262 nm, for use at a UV wavelength of 244 nm, is achieved by a two-stage etch. A scanning electron microscope photograph of a phase-mask plate is shown in Fig. 3.4. Generally, the phase mask is fabricated in small fields, which are then stitched together to form a long grating. Common problems with phase masks processed by e-beams have to do with inaccurate stitching of the fields. The positioning accuracy of the e-beam and variation of the silica mask plate height cause phase steps to occur between fields, and the resolution of the photoresist causes random variations in the individual periods of the grating. Techniques have been developed to minimize these errors [46,20]; however, the random variation in the absolute positioning of the e-beam is a fundamental limitation. Typically, the writing of long phase-masks by e-beam needs constant referencing and correcting owing to small temperature variations during the exposure period, which may last several hours. These problems are of greater importance as the length of the grating increases. Phase masks as long as 120 mm have been reported [22], although the quality of the fabricated Bragg grating has not been reported in detail. Stitching is not an issue when the alternative technique of holographic phase-mask fabrication is used. This technique is, in principle a superior method for phase-mask production. However, long phase masks have been difficult

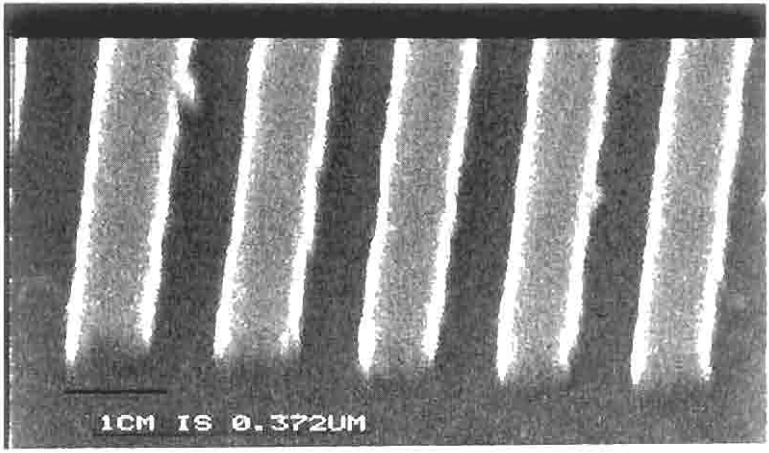

Figure 3.4: SEM photograph of a high-quality phase mask used for grating inscription of ~1060-nm Bragg gratings. (Courtesy Ian Lealman, BT Labs)

to produce holographically, owing to problems with uniformity of illumination and the requirement for large mirrors. Lenses can be used to alter the phase front of one of the interfering beams to allow the fabrication of *continuously* chirped gratings, as opposed to step-chirped gratings by e-beam fabrication [23]. Since the fabrication of the holographic phase mask depends on geometrical alignment of interfering beams, the mass production of identical phase masks may remain a problem.

3.1.3 The phase mask interferometer

UV lithographic replication has been used extensively to fabricate phase masks directly in silica plates using e-beam writing and plasma etching [24], to function as lenses and complex spatial elements. This technique has also been applied successfully to fiber Bragg grating inscription and reported in the literature by several laboratories at around the same time [25–28]. There are several methods of using the phase mask: as has been stated, it may perform the function of simple beam splitting in the interferometer in Fig. 3.1. So why is it such a useful element, when a far cheaper dielectric beam-splitter can be used instead? Its primary aim is to be used simply as a wavelength-*defining* element in an interferometer (as shown in Fig. 3.5); used as a beam splitter with the beam-combining mirrors (Fig. 3.5) to adjust the wavelength of the fiber grating.

The change in the Bragg wavelength as a function of the change in the mutual angle between the two interfering beams as shown in Fig. 3.5 is found by substituting Eqs. (3.1.3) and (3.1.4) into Eq. (3.1.1) and differentiating with respect to θ:

$$\frac{\Delta\lambda}{\lambda_{Bragg}} = -\frac{\Delta\theta}{2}\cot\frac{\theta}{2}. \tag{3.1.5a}$$

Figure 3.6 shows the Bragg wavelength in the fiber as a function of the half-writing angle. With the diffraction angle fixed at ~10° (phase mask for ~1550 nm), a change of 5° alters the Bragg wavelength by ~800 nm [29]. The enormous tunability of this interferometer, as well the ability to find a reference position for the phase-mask Bragg wavelength, makes it highly flexible. It requires a single-phase mask, which is used as both a beam splitter *and* a Bragg wavelength reference. It can also be used to replicate chirped phase masks, and a tunability of the Bragg wavelength of ~250 nm has been demonstrated [29].

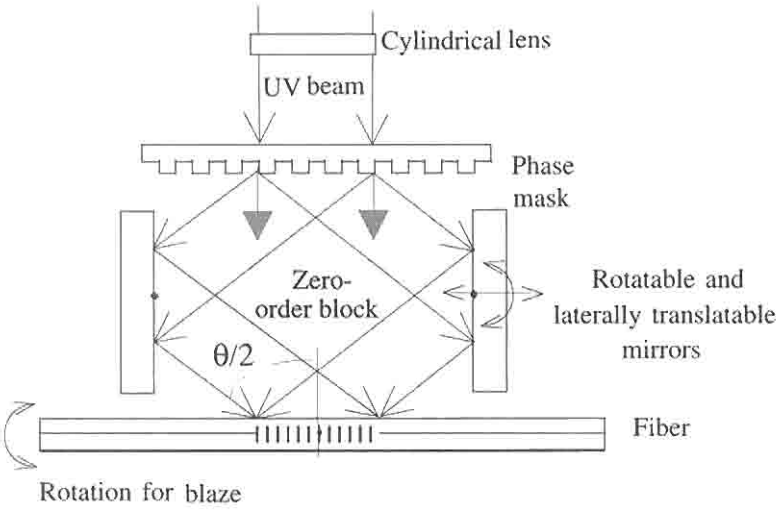

Figure 3.5: The phase mask used as a beam splitter in an interferometer for inscription of fiber gratings. The phase mask predefines the wavelength of the reflection grating, when the mirrors are at right angles to the axis of the fiber and the phase-mask plate (Talbot interferometer) [see Eq. 3.1.3 and 3.1.4]. In this scheme, the paths of the two interfering beams are identical, making the interferometer suitable for use with low-spatial-coherence sources.

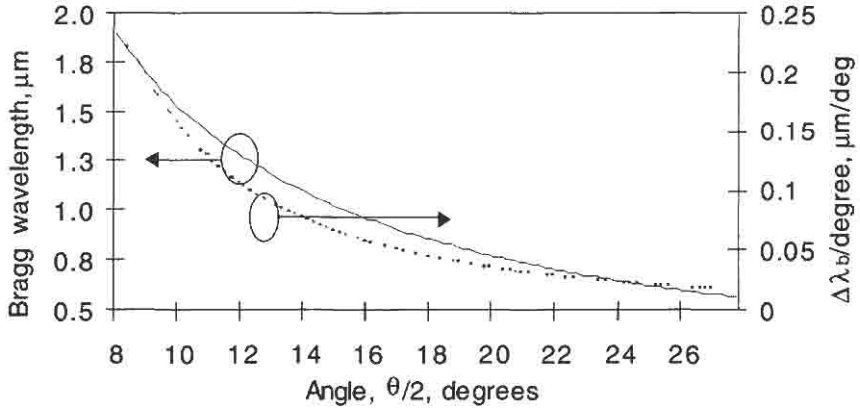

Figure 3.6: The Bragg wavelength (dashed curve) and the rate of change of the Bragg wavelength (continuous curve) as a function of the phase-mask diffraction angle. A change of ~1.6° around a mean diffraction angle of 10° is equivalent to a change in the Bragg wavelength of ~250 nm.

Alternatively, the fiber may be placed directly behind the phase mask for photo imprinting of the grating. In this scheme, there are two important issues. First, since the diffracted beams interfere in the region of overlap immediately behind the phase mask, the fiber core needs to be at the phase-mask surface for maximum overlap. The closest the phase mask can be placed to a fiber core is a distance equal to the fiber radius (unless a "D-fiber" is used), which means that there is no overlap of the two beams in a short region at either end of the grating. Second, the interference pattern generated at the fiber core is the sum of the interference of *all* the diffracted orders. For a pure sinusoidal pattern at the fiber core, it is important to allow only the two ± 1 orders to interfere with the zero-order suppressed. As has been observed with the phase mask in contact with the fiber, even with a zero-order nulled phase mask, the period of the imprinted grating depends strongly on the intensity of the writing UV beam. At low intensities, the period is half the phase-mask period [see Eq. (3.1.3)], but at high intensities, even a low zero-order intensity can interfere with the ± 1 orders to create a grating of the same period as the phase mask itself [120]. Tilting the fiber at an angle α behind the phase mask so that one end is further away shifts the Bragg reflection to longer wavelengths as the inverse of cosine α, since the fringe planes are no longer orthogonal to the propagation axis. This method for tuning the Bragg wavelength has been demonstrated [30]; it should, however, be remembered that the grating length shortens with tilt, and not only does the reflectivity drop (due to limited coherence of the UV source), but radiation loss can increase [41] (see Section 3.1.4).

The zero-order beam may be avoided by repositioning the mirrors. This is shown in Fig. 3.7a, where the grating is written at a point well removed from the incident zero order. The path length of the two interfering beams remains identical. A similar result may be achieved by tilting the beam-folding mirrors by an angle α from the perpendicular to the horizontal plane. On reflection from the surfaces, the beams are directed at angles of 2α to the horizontal plane, out of the plane of the zero-order beam, as shown in Fig. 3.7b.

It is usual to place a cylindrical focusing lens before the phase mask in the path of the UV beam so as to allow two stripes (within the plane of the paper in Fig. 3.7a) to overlap at the fiber. This has the advantage of focusing in one plane and increasing the power density, while leaving the length of the grating unaltered. Care need to be taken in adjusting

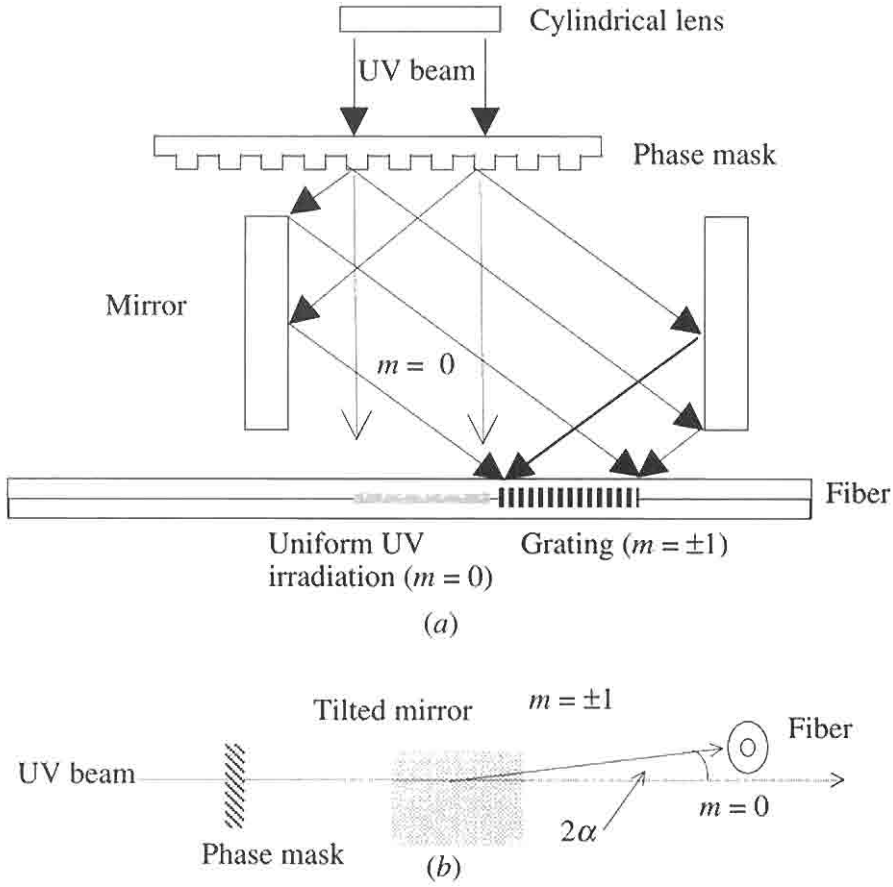

Figure 3.7: (a) Avoiding the zero order from the region of the grating by repositioning the interferometer mirrors. Alternatively, tilting the mirrors outward from their normally vertical positions, means that the beams no longer interfere in the plane of the zero order (b).

this interferometer, since the orientation of the phase mask determines whether the two beams will overlap at the fiber, while the cylindrical lens determines whether or not the overlapping stripes align along the fiber core. It is important to ensure that the path lengths from the phase mask to the fiber are identical so that the mutual coherence of the beams is

maximized [31]. The fiber should be placed in the region of the fringes such that the propagation axis is normal to the fringe planes, since any angular misalignment increases radiation loss from the light propagating in the fiber (see Chapter 4) and shifts the Bragg wavelength.

If mutual counterrotation of the mirrors is incorporated in the phase-mask interferometer, grating inscription becomes infinitely flexible with a *single* phase mask. Two modifications are required if Bragg wavelength tunability is required: the mirrors need to be rotated, and the distance of the fiber from the phase mask must be changed. Using a translation stage to hold the fiber *in situ* easily incorporates the latter. The alignment of the interferometer is simply and quickly carried out by using a borosilicate glass microscope coverslip to view the fluorescence of the individual UV beams. The coverslip is moved toward or away from the interferometer until the fluorescence from the two beams overlaps. The fiber simply replaces the glass slide for grating inscription. Figure 3.8 shows a photograph of the fully flexible interferometer in use at BT Laboratories.

The polarization of the UV laser beam affects the inscription of the grating in the fiber [32–39]. To ensure that the inscribed grating has low polarization sensitivity, the polarization of the UV laser beam should be oriented parallel to the propagation axis of the fiber [40]. (Gratings inscribed with UV laser radiation polarized orthogonal to the propagation direction show significant birefringence due to effects of induced birefringence.) This may be achieved by placing an appropriately oriented half-wave plate before the phase mask.

Replacement of the two mirrors in Fig. 3.5 by a rectilinear UV transmitting silica block [23] results in an extremely compact and stable interferometer. The diffracted UV beams enter a face of the silica block and are totally internally reflected by adjacent sides to emerge through the opposite face, interfering at the fiber. The beam paths are shown in Fig. 3.9.

The silica block is placed halfway between the phase mask and the fiber. The maximum grating length, which can be written in a fiber is related to the dimensions of the block. The length L_g of the grating is a function of the length of the side of the silica block (mirror) as

$$L_g = L_s \tan\left[\sin^{-1}\left(\frac{\sin(\theta_m/2)}{n_s}\right)\right], \tag{3.1.6}$$

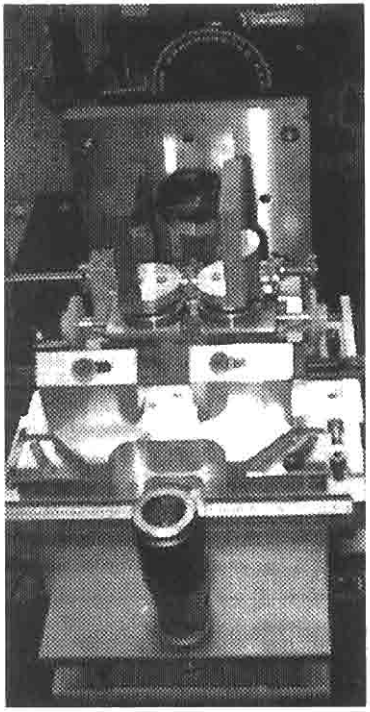

Figure 3.8: The photograph shows the tunable phase-mask interferometer. The distance between the mirrors can also be altered without misaligning the interferometer. The fiber can also be rotated around the vertical axis to allow the inscription of slanted gratings (see Section 3.1.4).

where n_s is the refractive index of the silica block at the writing UV wavelength. Assuming that $\sin \theta_m/2 \approx \theta_m/2$ for small angles, the maximum length of the grating, which may be written with a side of L_g is

$$L_g \approx \frac{L_s \theta_m}{2n_s} \approx \frac{L_s \theta_m}{3} . \tag{3.1.7}$$

For fiber Bragg gratings at a wavelength of 1500 nm, the angle $\theta_m/2 \sim 10°$; the length of the silica block side is then approximately 17 times the grating length. The minimum width of the silica block W_s is equal to the grating length L_g without in-line zero-order suppression. However, if the zero order is to be physically blocked by an opaque element,

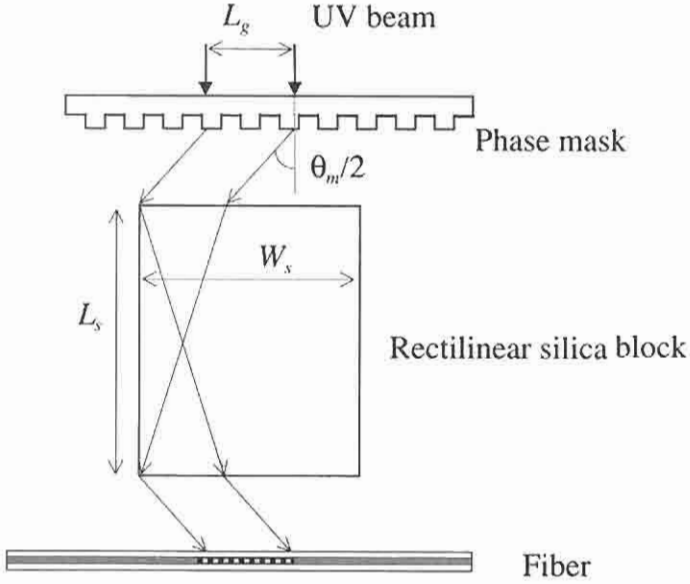

Figure 3.9: Replacement of the two mirrors in Fig. 3.5 by a UV-transmitting silica block. Only one set of diffracted UV beams is shown for simplicity.

then the width $W_s \geq 3L_g$. This width is reduced to $2L_g$ if the interferometer in Fig 3.5 is used with the zero-order beam block halfway in between the mirrors. For long gratings the dispersion of the silica block is a limitation if the interferometer is used with a low-coherence source. However, simplification of grating inscription makes this setup highly attractive.

There are many advantages of using a phase mask. It allows the wavelength of the fiber grating to be defined precisely for replication. Matching fiber grating reflection wavelengths is made easier, since the phase mask is the interferometer itself. Mass production of identical fiber gratings is thus possible. Another advantage of the phase mask is that a predetermined function may be inscribed in it for replication into the fiber [23] (see Section 3.1.13). The phase mask forms a very stable interferometer since there are no adjustable parts, allowing long inscription times. It is also insensitive to the translation of the inscribing UV beam and tolerant to beam-pointing instability of the laser beam. The advantage of translation insensitivity allows long fiber gratings to be written by the scanning technique, discussed in Section 3.1.5. Disadvantages of using

the phase mask nearly in contact with the fiber are the dangers of contamination and permanent damage of the phase mask. A different phase mask is required for each specific Bragg wavelength. This need not a problem, since several gratings can be written on a single phase-mask plate, each at the required wavelength [41]. Alternatively, a tunable interferometer can be used with a single phase mask; however, it does require careful calibration and alignment.

3.1.4 Slanted grating

If the fiber is tilted out of the plane of Fig. 3.5, the grating inscribed in the fiber will be slanted in the direction of propagation of the mode. This, however, requires the interfering beams to have a large cross-sectional area so that the beams may overlap, as shown in Fig. 3.10a. This is inconvenient for most interferometers, since the cylindrical lens focuses the beams *in the plane* of the figure, unless the unfocused beam intensity is already high. An alternative and simple method for inscribing slanted gratings is to tilt the fiber in the plane of the figure, as shown in Fig. 3.10b [41]. In this case, the coherence properties of the laser will determine the visibility of the fringes at the fiber. Since the fiber is at an angle to the incoming beams, the inscription of the grating depends on the overlap of the two beams and is slightly shortened; the depth D of the fringes for the interferometer shown in Fig. 3.10b is

$$D \leq \frac{W}{\tan(\theta_m/2)}, \tag{3.1.8}$$

where W is the width of the normally incident UV beam and $\theta_m/2$ is the diffraction angle shown in Fig. 3.3. Figure 3.11 shows the depth of the fringes and the overlap of the beams. For small tilt angles α, the period Λ_s of the slanted grating in the direction of propagation varies as

$$\Lambda_s \approx \frac{\Lambda_g}{\cos\,\alpha}. \tag{3.1.9}$$

The fringe pattern shown in Fig. 3.3 is unchanged; however, since the fiber core is at an angle to the fringes, a grating, which is blazed with respect to the propagation direction of the mode, is formed. These gratings have special applications as lossy filters and are discussed in Chapters 4 and 8. In Fig. 3.14, the extent of the fringes formed in the overlap region

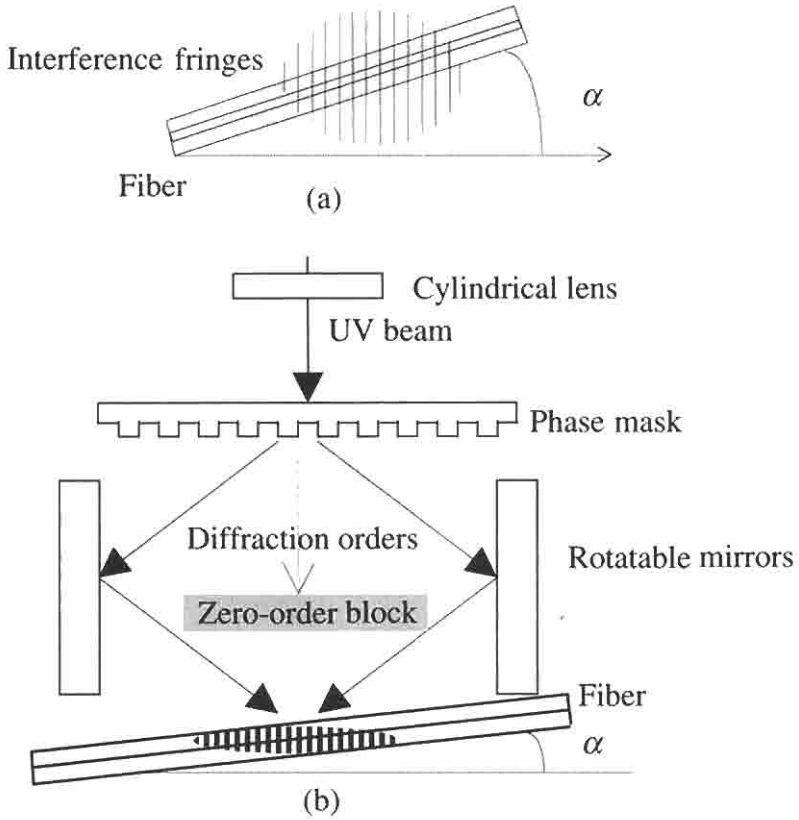

Figure 3.10: (a) The fringes formed at the point of intersection need a large cross-sectional area for a slanted grating to be written in the fiber. Shown in (a) is view of the fringes in a plane normal to the zero-order, and α is the rotation angle in that plane. (b) shows another method for writing slanted gratings, in the plane of the incoming beams [41]. The fiber is rotated by an angle α within the plane of the beams such that it overlaps with the interference fringes; the coherence properties of the UV source as well as the depth of fringes determine this.

is shown. The maximum possible fringe depth D is indicated in Fig. 3.11. Coherence, both temporal and spatial, limits D to less than this value, as described in Eq. (3.1.8). For a phase mask used in near contact with the fiber, the depth of the fringes is less than $D/2$.

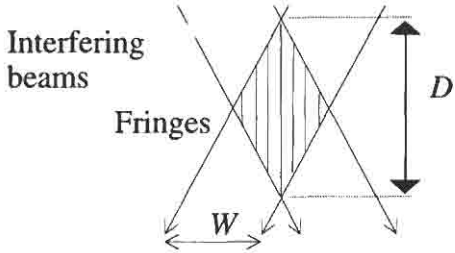

Figure 3.11: The overlap of the two interfering beams forms a diamond figure, with a depth of the fringes D. The grating length varies depending on the placement of the fiber within the fringes.

3.1.5 The scanned phase mask interferometer

Figure 3.12 shows how the phase mask may be scanned for inscribing long gratings into fibers. This technique was first demonstrated by Ouellette *et al.* [42]. It was shown that 19-mm long gratings may be faithfully reproduced in fibers; a slight nonuniformity in the phase mask was also removed by applying a temperature gradient across the fiber length after writing the grating. Byron *et al.* [43] reported a 50-mm long grating in which the quality of the interferogram was varied by adjusting the intensity of the writing beam along the length of the grating. This method allows the tailoring of the transfer characteristics of the fiber grating and

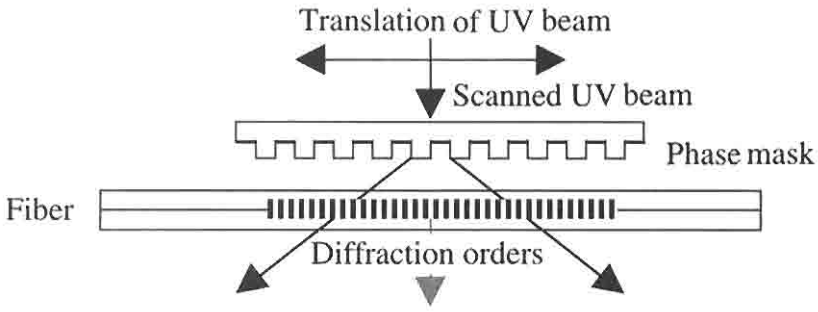

Figure 3.12: The phase mask used as a scanned interferometer is a powerful method of fabricating long-fiber gratings. The quality of the grating is dependent on the uniformity of the phase mask.

will be discussed in Chapter 5. The length and the quality of the phase mask limit the scanning technique. With the best e-beam facility, the absolute positional accuracy is around 5 nm. This positional error sets the limit on the stitching of the fields. Although the error is random and the effects are averaged out over the length of the mask [44], the stitching errors are manifest in the transfer characteristics of the grating [45]. This causes multiple reflections and structure within the reflection envelope determined by the field size, while the reflection bandwidth is inversely dependent on the overall length of the grating. Techniques have be applied to reduce the effects of stitching errors in phase masks by altering the field size of each subgrating processed by the e-beam. By overlaying N e-beam exposures with different field sizes, each with $1/N$ of the dose, the total dose required to imprint the grating pattern in the photoresist on the phase mask is maintained while averaging out the periodic nature of the stitching errors. Developing the resist dramatically reduces the effects of the stitch errors, which appear as multiple out-of-band reflections. This has been successfully demonstrated [46], and the effects on the reflection spectrum are shown in Fig. 3.13.

Another technique, albeit used less successfully, monotonically increased the field sizes for a 14-mm long grating, from 100 μm to 200 μm in steps of 1.055 μm. Although many of the features were eliminated, field sizes around 200 μm produced a cluster in the reflection spectrum [46], since the fractional change in the field-size remains small.

Stitching errors or undesirable chirp in a phase mask are replicated in a fiber grating. It is possible to use the technique of "UV trimming" [47] to adjust the local refractive index in the fiber to correct the transmission spectrum. Scanning a UV beam across a phase mask while also moving the fiber, enables the chirp in the phase mask to be compensated for [48,49]. By adjusting the velocity of the fiber relative to the scanning UV beam at different positions along the phase mask, the induced refractive index change can be changed, altering the local Bragg wavelength. If the phase mask has an unintended chirp, the fiber grating can be "trimmed." This technique has been applied to reduce the chirp of a grating written by using a 100-mm long phase mask that had undesired chirp situated close to the middle of the mask. This was found by monitoring the growth of the reflection of a grating. The velocity is adjusted in steps (5 sec to 22 nm/sec) with the help of a piezoelectric stage, while the UV beam is scanned at a velocity of 250 μm/sec during fabrication of a second grating. The induced wavelength shift is directly related to the velocity of the

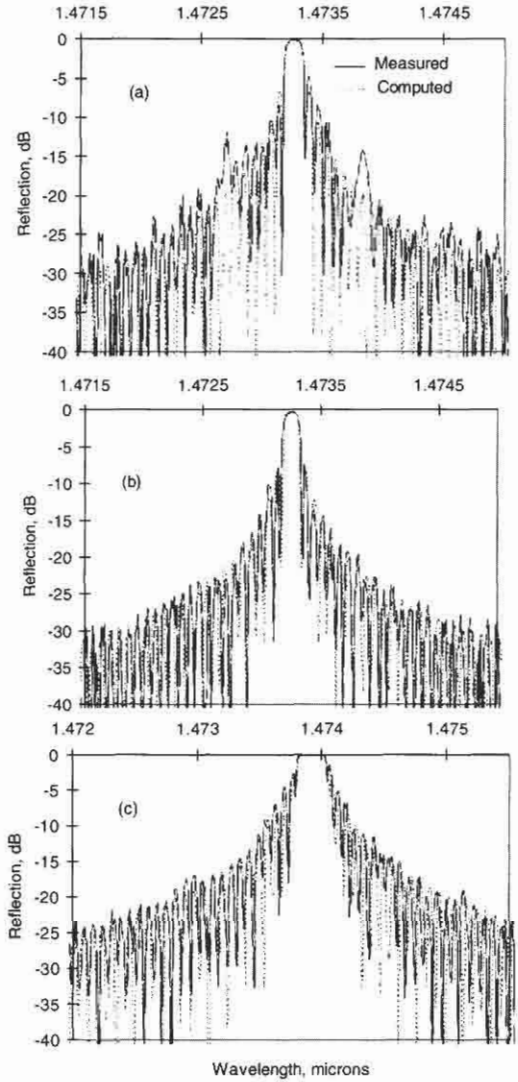

Figure 3.13: Reflection spectra from imprinting with different phase masks as a function of the number of overlaid e-beams exposures of the phase mask. This grating is discussed in Section 3.1.13. (a) Single-pass field size of 65 μm; (b) three passes with 65.4, 55.3, and 59.26 μm; (c) as for (b) with additional 66.04 μm pass (from: Albert J, Theriault S, Bilodeau F, Johnson D C, Hill K O, Sixt P, and Rooks M J, "Minimisation of phase errors in long fiber Bragg grating phase masks made using electron beam lithography," *IEEE Photon. Technol. Lett.* **8**(10), 1334–1336, 1996. © 1996 IEEE [46]).

scanning beam v_{uv} and that of the fiber v_f as $\Delta\lambda = \lambda v_f / v_{uv}$. Removal of the chirp reduced the bandwidth of the grating from 0.23 nm to 0.1 nm [48].

The elimination of out-of-band ghosts is important for telecommunications, while the postfabrication repair of expensive phase masks is very useful for fabrication.

3.1.6 The Lloyd mirror and prism interferometer

In the double mirror arrangement of the interferometer shown in Fig. 3.1 the incident beam is split into two, and fringes form from interference between identical copies of the incident radiation. Any phase distortion across the input beam is automatically compensated for at the fringe plane, or can be compensated for by the introduction phase plates, so that local visibility of the fringes remains close to unity and chirp in the period of the fringes reduced to zero.

Figure 3.14 shows an arrangement for an interferometer based on a single mirror known commonly as the Lloyd mirror. A parallel beam

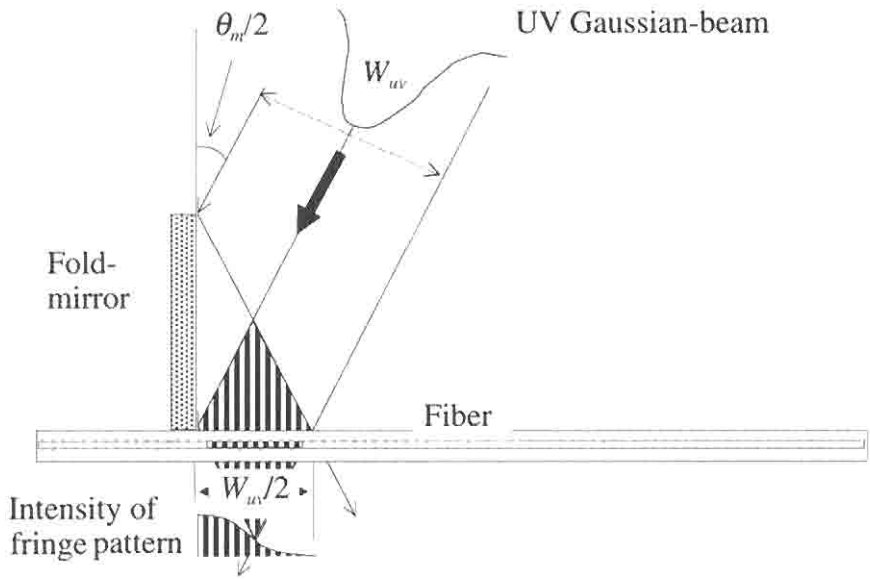

Figure 3.14: The Lloyd mirror interferometer, showing the intensity of the fringes formed at the fiber with a folded Gaussian beam [50].

incident at the surface of the mirror at a shallow angle is reflected across the path of the beam. Interference occurs in the region of overlap of the reflected and unreflected parts of the incident beams. The interferometer is therefore extremely simple and easy to use. However, since half of the incident beam is reflected, interference fringes appear in a region of length equal to half the width of the beam. Secondly, since half the beam is folded onto the other half, interference occurs, but the fringes may not be of high quality. In the Lloyd arrangement, the folding action of the mirror limits what is possible. It requires a source with a coherence length equal to at least the path difference introduced by the fold in the beam. Although a phase plate may be used over half the beam to compensate, experimentally this is not straightforward. Ideally, the intensity profile and coherence properties should be constant across the beam; otherwise, the fringe visibility will be impaired and the imprinted grating will be nonuniform. Since most sources tend to have a Gaussian beam profile, it is difficult to produce fringes which have a uniform transverse profile. The grating profile remains half-Gaussian, unless the beam is expanded to provide a more uniform profile. The Gaussian intensity profile of the fringes introduces a chirp in the imprinted grating. Diffractive effects at the edge of the mirror may also cause a deterioration of the fringes closest to it.

The Lloyd arrangement with the single mirror is easy to tune. However, the fiber axis should be placed orthogonal to the plane of the mirror so that the grating is not slanted.

Replacement of the mirror by a prism in the Lloyd arrangement results in a more stable interferometer. This is shown in Figure 3.15. The UV writing beam is now directed at the apex of a UV-transmitting silica right-angled prism such that the beam is bisected, as in the Lloyd mirror. Both halves of the UV beam are therefore refracted and no longer travel in air paths, which can change with time.

The interferometer thus becomes intrinsically stable and was used to produce the first photoinduced fiber Bragg gratings in the 1500-nm wavelength window [51]. The interferometer has been used to demonstrate a distributed-feedback dye laser. Interfering the pump beams in the dye at the appropriate angle to create a Bragg reflector (absorption grating) caused the dye to emit laser radiation [52].

The advantages and disadvantages of this interferometer are similar to those of the Lloyd mirror. However, there are two further points of interest. Owing to the shallow angle subtended by the UV beam on the hypotenuse, the prism face has to be much larger than the beam width,

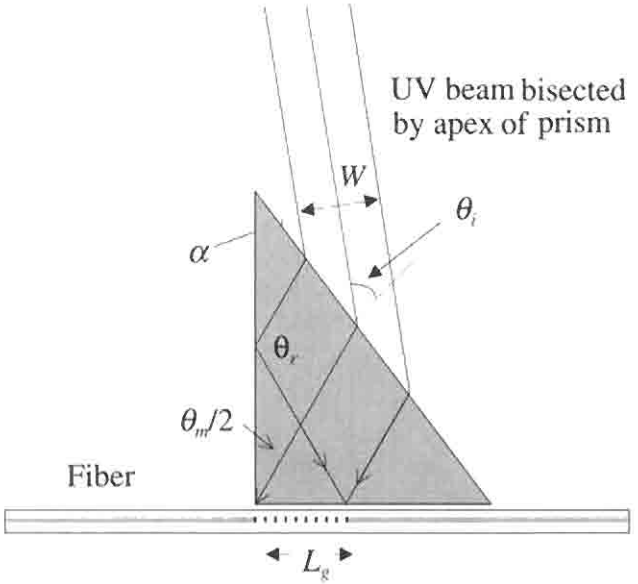

Figure 3.15: The Lloyd prism interferometer. The interfering beam paths are within the bulk of the prism; however, there is a path difference introduced between them due to the refractive index of the prism. The UV beam must be spatially and temporally coherent with a uniform intensity for the production of high-quality gratings.

but because of refraction, the side of the prism at which total internal refraction occurs is smaller than the length of the Lloyd mirror [see Section 3.1.3, similar to Eq. (3.1.6)]. For a given beam width, the prism interferometer expands the length of the grating, and this is shown in Fig. 3.16. Using simple geometry, the length of the grating L_g may be shown to be

$$L_g = \frac{W}{2 \cos \theta_i} \left[\sin \alpha + \cos \alpha \tan\left(\frac{\theta_m}{2}\right) \right], \qquad (3.1.9a)$$

the parameters for which are defined in Fig. 3.15.

At large angles of incidence (small apex angles), the grating length increases rapidly but reflection losses increase at the same time. The polarization useful for writing a grating with low birefringence (p-polarized) is reflected more than the unwanted polarization (s-polarized) [40] [see Section 3.1.8]. Antireflection coating of the surface will naturally

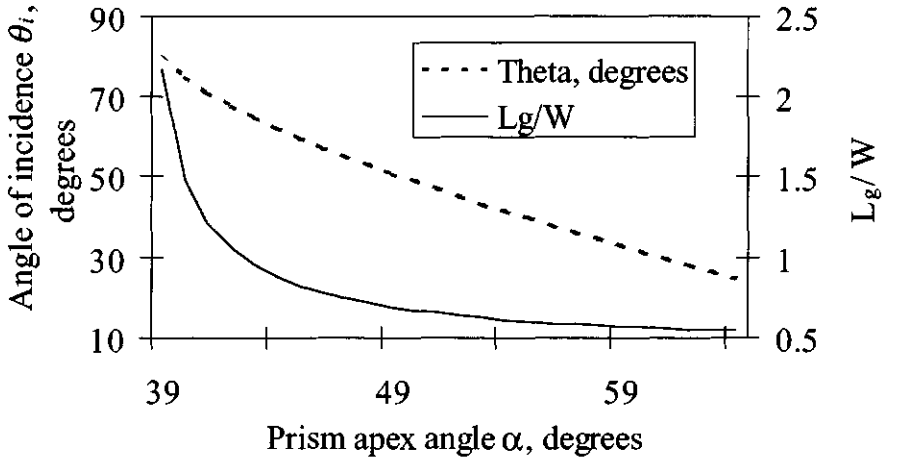

Figure 3.16: Length of a grating normalized to the width of the UV beam as a function of prism apex angle α. The writing angle $\theta_m/2$ is fixed at 10° for a Bragg wavelength of ~1500 nm. Also shown is the external writing angle of incidence on the surface of the prism, θ_i. Note that since the beam is folded about the center, the grating length is approximately half the width for the Lloyd mirror, whereas with the prism, the grating can be longer.

reduce this loss. Dispersion in the silica prism may also be an issue when writing gratings longer than a few millimeters.

Other techniques for the production of gratings with a single prism in a slightly modified version of that shown in Fig. 3.15 have also been reported [53,54]. These methods require precision-fabricated prisms and are restricted in tunability of the Bragg wavelength but may prove to be useful in cases where a rudimentary inscription procedure is necessary.

3.1.7 Higher spatial order masks

According to Equation (3.1.4) the period of the mask may be integer multiples of the Bragg wavelength. It is therefore possible to use a coarser grating period than the fundamental period required for the reflection wavelength. As the period gets larger, it is not practical to use the phase mask as a diffraction element, and it is necessary to use an amplitude mask for direct replication of the grating. The larger periods also allow the photoreduction of the mask using imaging to imprint the correct period

grating in a fiber [55,56]. The latter scheme requires the higher-order mask to be $M \times$ the length of the photo-reduced grating, where M is the demagnification factor, posing a problem for the production of fiber gratings that are longer than a few millimeters. The projection scheme enables the production of gratings with a single 20 ns pulse from a KrF excimer laser at a wavelength of 248 nm.

One- to six-micron period gratings have been produced by projection of an amplitude mask with multilayer stacked high-reflectivity dielectric stripes as the pattern (5 to 120 μm wide stripes). An image demagnification of 1:10 was used with 0.3NA optics to produce 4-mm from long gratings of 6th, 11th, and 12th order. Reflectivities as high as ~70% were noted for the lower-order gratings with correspondingly lower reflectivities of 8 and 2% for the 11th and 12th orders, respectively. An advantage of the projection system is that the fluence at the fiber is increased by the demagnification, reducing the power density at the mask plate [56]. Also noted was the imprinting of a physical grating on the surface of the fiber cladding, penetrating some 2 μm into the cladding. A threshold for the production of the grating in the core at ~0.8 J/cm^2 was observed, while 1.4 J/cm^2 was required for optimal production of the grating. It appears that the physical damage grating in the cladding produces a phase grating in the core due to heavy surface modification, causing light to be scattered out of the core. Gratings formed by physical damage, known as Type II, will be discussed in Section 3.2.

A similar technique of photoreduction can also be applied for the projection of a phase mask and is shown schematically in Fig. 3.17. Projection of the phase mask rather than the amplitude mask overcomes the problem of the Rayleigh-limited resolution for the 0.3NA UV transmitting lens used in a photoreducer. The limit with the amplitude mask is 0.6 μm. It therefore cannot be used for the production of first-order gratings [55] with periods of ~0.5 μm. Disadvantages of the projection scheme for use with both the amplitude and phase mask are the requirement of large-scale high-quality UV-grade spherical optics, and the use of large-area amplitude and phase masks. The additional cost and complexity of the projection system may well offset the cost advantage of using coarser features.

A 10.66-μm period phase mask has been photoreduced by $\times$10 to generate first-order gratings in a Ge-doped fiber at a Bragg wavelength of 1530 nm. It was reported that the production of damage type II gratings was more reproducible using the phase-mask projection scheme [55].

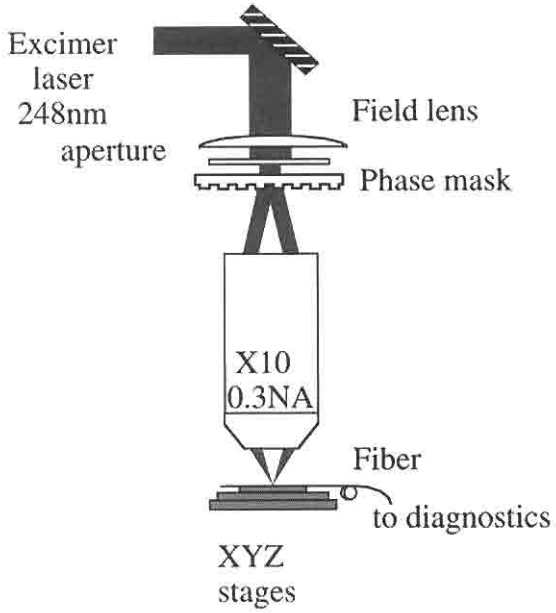

Figure 3.17: The projection system used to photoinscribe gratings by the photoreduction of the phase-mask (from Rizvi N H, Gower M C, Godall F C, Arthur G, and Herman P, "Excimer laser writing of submicrometre period fiber Bragg gratings using a phase-shifting mask projection," *Electron Lett.* **31**(11), 901–902, 1995, © IEE [55]).

Observation of higher-order interactions is possible with a first-order phase mask. This is simply governed by Eq. (3.1.4). A grating written for a Bragg wavelength λ_{Bragg} in first order will also operate at wavelengths $\lambda = \lambda_{Bragg}/N$. Additionally, if the grating imprinted in the fiber has a nonsinusoidal amplitude profile, for example, by effects of saturation of the refractive index modulation or physical damage (e.g., square wave modulation amplitude), then the grating will have Fourier frequency components at multiples of the first order, as $\Lambda = \Lambda_g/m$ (m = 1,2,3 . . .). These will in turn affect the efficiency of the reflections at shorter wavelengths, but function as *first*-order gratings for the Bragg wavelengths matching each of the spatial harmonic frequencies.

High-intensity UV printing through a phase mask results in multiple-order reflections, not least by the interference of the zero-order beam

through the phase mask with the ±1 orders, but also due to the formation of a damage grating which is no longer sinusoidal in amplitude [120].

3.1.8 Point-by-point writing

The period of a reflection grating operating at 1.5 μm is ~0.5 μm, as per Eq. (3.1.3). Since a diffraction-limited spot size of radiation at 244 nm is ~0.25 μm, it is possible in principle to form a periodic refractive index grating by illuminating a single spot at a time using a point-by-point writing scheme. Technically, using positioning sensors linked to an interferometer, a grating of such periods can be written. This is only suitable for short gratings, since it is difficult to control translation stage movement accurately enough to make point-by-point writing of a first-order grating routinely practical. Other methods, including the use of a phase mask or the multiple-printing in-fiber-grating scheme, are better suited to writing long first-order gratings. However, high-quality high-order gratings have been demonstrated for $N = 3$ and 5 [57]. While excellent reflection gratings can be written using other schemes, point-by-point writing is extremely useful for fabricating gratings of long periods (>10 μm). These gratings couple light from one propagating polarization mode to another in the backward [58] or forward direction as in a rocking filter [59–61] (discussed in Chapters 4 and 6), to forward-propagating radiation modes (also see Chapter 4), or from one guided mode to another [62–64]. Figure 3.18 shows the technique used for point-by-point writing of reflection gratings and polarization couplers. For the simple reflection grating, the fiber is illuminated by a tightly focused spot through a mask for the required duration before being translated by a motorized micropositioner for the next illumination. In this way, a reflection grating of any order may be written. Naturally, the method benefits from the use of a pulsed laser, since the motion of the fiber can be stepped without the need to control the operation of the laser as well. However, the method is most useful for long-period gratings, which do not require such a demanding positional accuracy.

3.1.9 Gratings for mode and polarization conversion

Polarization mode converters may be fabricated in birefringent fibers using this scheme. In this case, it is necessary to orient the birefringent axes of the fiber at 45° to the illuminating beam. Two methods have been

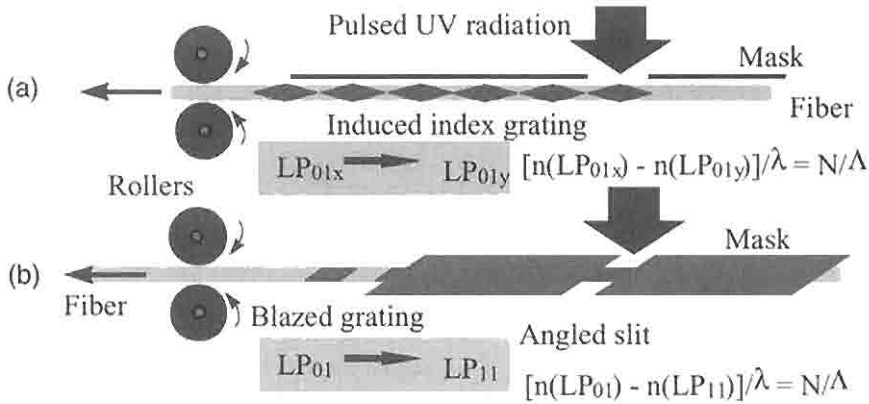

Figure 3.18: Point-by-point writing of fiber gratings. (a) shows a uniform grating being written as the fiber is pulled forward. A focused beam from a pulsed laser illuminates the fiber through a slit. The fiber pulling speed and the laser pulse-rate determines the period of the grating. (b) Blazed gratings are written with a slanted mask. Coupling between dissimilar modes is therefore possible (after Ref. [57]).

demonstrated to form such polarization converters. In order to use a *non*birefringent standard telecommunication fiber for a polarization mode converter, it must be made birefringent. The fiber can be wrapped on a cylinder of an appropriate diameter to induce a specific birefringence [65]. The beat length of the modes in the fiber is a function of the bend-induced birefringence and may be changed by altering the diameter of the cylinder. The induced birefringent axes are along the radius and parallel to the surface of the cylinder, with the fast axis in the radial direction. The induced birefringence B is [66]

$$B = n_{fast} - n_{slow} = -\alpha\left(\frac{d_{fiber}}{D_{cylinder}}\right)^2, \tag{3.1.10}$$

where d_{fiber} and $D_{cylinder}$ are the diameters of the fiber and cylinder, respectively, and the fast and slow axis refractive indices n are indicated by the subscripts. α is a constant that is dependent on the photoelastic properties of the fiber material, ~0.133 for fused silica.

Typically, the induced birefringence in fibers wrapped around the smallest practicable diameter cylinders ($D_{cylinder} \sim 25$ mm), based on consideration of mechanical strength, is of the order of -2×10^{-6}. While

this value is large compared to the intrinsic birefringence of standard telecommunications fiber, it is well below that of birefringent optical fibers (maximum birefringence $B_{max} \sim 0.4 \times \Delta n^2$, where Δn is the core cladding index difference [67]; for $\Delta n = 0.04$, $B_{max} \sim 6.4 \times 10^{-4}$). If a grating with a period, $\Lambda_g = \lambda/B$ is written in the fiber, then coupling between the two polarizations will occur. However, the grating has to be written oriented at 45° to the fast and slow axes. This may be done simply by arranging the UV illumination in a direction of the axis of the cylinder but rotated at an angle of 45° to the surface of the cylinder. As the fiber moves across the slit, the laser is switched on so that half the period of the grating is exposed to UV radiation before it is switched off for the second half. The process is repeated until the required number of periods is written [59]. Parameters that may be varied are the angle of inclination Ψ (known as the *rocking angle*), as shown in Fig. 3.19, and the mark–space ratio A_g of the grating given by the ratio of the length of fiber exposed to UV radiation and the grating period, in any one grating period.

A transversely uniform grating will promote coupling between modes of the same order whereas coupling of different-order modes requires a blazed grating [68] or, equivalently, a grating that is transversely nonuniform. A blaze may be imparted by rotating the mask slit so that the exposed region makes an angle to the propagation axis in the fiber, as shown in Fig. 3.18b. The blaze angle and the mark-space ratio $A_g = L_{exposed}/\Lambda_g$, are again parameters that may be adjusted to alter the performance of the filter. Blaze also enhances coupling to radiation modes of the fiber, inducing transmission loss, as has been mentioned in Section 3.1.4. However, the period of the grating Λ_g required to couple between modes is generally much longer than that required to couple to the radia-

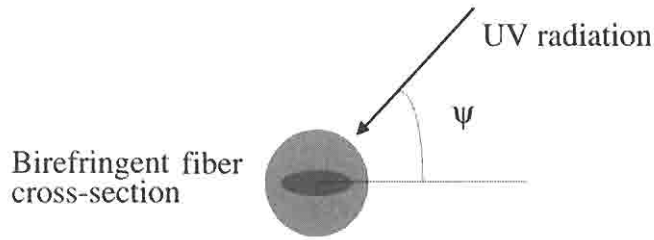

Figure 3.19: The rocking angle Ψ may be varied to alter the coupling coefficient for the filter.

tion modes in the counterpropagating direction. This is no longer true for coupling to copropagating radiation modes, and care needs to be taken to ensure that the periods of the gratings are not identical, by choosing an appropriate fiber. Intermodal coupling has been demonstrated using internally [62,69], as well as externally written gratings for different order mode coupling [61], as well as similar order modes [64]. The functioning of these devices is discussed in Chapter 6.

3.1.10 Single-shot writing of gratings

Single-shot writing of fiber gratings has been demonstrated using pulses from an excimer laser [118–121]. Higher reflectivity gratings have also demonstrated in boron–germanium codoped optical fiber [123]. Although the quality of these gratings has not been comparable with those written with other methods, the principle has led to a novel scheme of writing grating in the fiber while it is being drawn from a preform.

The process of writing a grating in an optical fiber generally requires the stripping of the protective polymer coating, which is opaque to short-wavelength UV radiation. Stripped fiber is weakened owing to mechanical processing (see Chapter 9) during grating inscription and should ideally be recoated. However, grating inscription on a fiber-drawing tower enables the fiber grating to be coated immediately after fabrication. Further, an array of gratings may be fabricated sequentially in a length of fiber by stepping the Bragg wavelength after each inscription. Figure 3.20 shows a schematic of grating fabrication during fiber drawing that was originally proposed by Askins *et al.* [122] and subsequently demonstrated [123]. Stepped-wavelength gratings were demonstrated using an interferometer that was tuned to a different Bragg wavelength between pulses from the excimer laser [122]. Although the gratings can be written during fiber drawing, the quality and repeatability remains poor, owing to problems of beam uniformity, mechanical alignment, and stability. For some applications in which a simple reflection is required, the quality of the grating may not be a critical parameter.

Advances in polymer coating materials have resulted in perfluorinated polymers that are essentially transparent in the longer UV wavelength regions of 266–350 nm [70,71]. Grating inscription at these wavelengths has been demonstrated as well, indicating that high-quality *and* high-reflectivity gratings may be possible without stripping the coating off the fiber. The fabrication of gratings in fiber with the primary

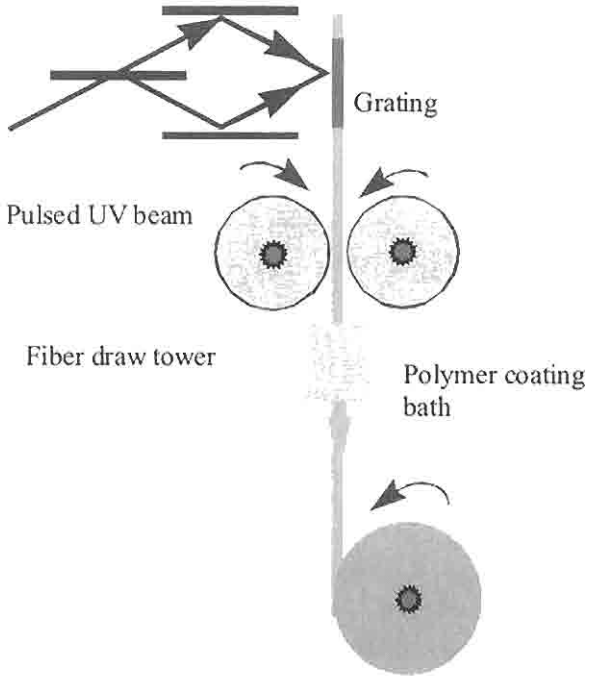

Figure 3.20: The scheme of writing gratings in a fiber while it is being drawn from a preform: 20-ns pulses at a wavelength of 248 nm were used to inscribe a sequential array of 50 gratings stepped at 0.1 nm. Also demonstrated were 120 gratings written at the same wavelength. The wavelength stability was good, but the peak reflectivity was ~3%. Gratings with a wavelength spacing of 5 nm were also reported [122].

coating may well be restricted to the use of CW UV sources, since high-power pulsed sources are likely to damage the polymer coating unless tight focusing is used to reduce the intensity at the surface [119].

3.1.11 Long-period grating fabrication

Long-period gratings have found applications as lossy filters. These gratings couple the guided and the radiation modes in the copropagating direction, and typically require periods in the region of 100 to 500 μm. LPGs are therefore most conveniently fabricated by UV exposure through a shadow mask [72]. These gratings tend to be longer than reflective Bragg gratings (tens of millimeters) since the periods are a few hundred

times longer. However, shadow masks are easily available, and the inscription requires simple contact printing as with the phase mask, but without the complexity of interferometry. Point-by-point writing is also possible.

Long-period amplitude masks have been patterned on dielectric mirrors to reduce the problem of optical damage with excimer lasers. In this application, a dielectric mirror coated with photoresist was first exposed to an amplitude pattern using a UV laser. The photoresist was developed to expose the dielectric mirror, which was then etched in 5% HF solution in deionized water. The resultant mirror had stripes at the required period for the LPG. Exposure through this mirror only allows the UV radiation to be transmitted through the regions where the mirror has been etched away. These mirrors were shown to withstand 200 mJ/cm^2 per pulse over several pulses, thus making them better suited for use than chrome-coated silica masks with an average damage threshold of ~50–100 mJ/cm^2 [131].

3.1.12 Ultralong-fiber gratings

To circumvent the limitations of the finite length of the phase mask, several techniques have been proposed to fabricate gratings of arbitrary length >200 mm [49, 73–75]. The simplest method is to sequentially inscribe gratings in a fiber from a phase mask of length L, to result in a grating with a length equal to the number of sequential inscriptions $\times L$ [74]. This is a powerful technique, which has special applications in the fabrication of long chirped gratings and is discussed in Section 3.1.15.

A technique based on the principle of inscribing small, more elementary gratings to create a longer one has also been reported [73]. The principle of inscription may be understood as follows: A short (4 mm) interference pattern is printed periodically in a continuously but slowly moving fiber. Using a pulsed laser (20-ns pulses), a 4-mm long section is imprinted in the fiber at any one time. The velocity of the fiber is such that within the pulse width, it may be regarded as being stationary. When the fiber has moved a few integral numbers of grating periods, a second pulse arrives, imprinting yet another grating partially overlapped with the previous grating but adding a few extra periods to the length. A mini–Michelson interferometer operating at 633 nm is attached to the moving fiber platform to track its position relative to the interference fringes. The latter is undertaken by the use of serrodyne control [73]. The resulting gratings have the narrowest reported bandwidths of 0.0075 nm,

although the quality of the grating was not perfect. It is important to eliminate stitching errors between the imprinted fields, as in the case of the phase mask, requiring a positional accuracy of better than 0.1Λ over the length of the grating. As an example, this implies maintaining an overall positional accuracy of less than 50 nm over the entire length of the 200-mm long grating, a demanding task.

Figure 3.21 shows the apparatus used for writing long gratings by the multiple printing in fiber (MPF) technique [73]. The fiber is held in a glass V-groove along its entire length and translated along the pulsed interference fringes in sychronym with the pulses. By moving the fiber at a constant velocity with a *linear* motor, the vibrations common in stepper-motor-driven systems are eliminated. Mounting the fiber carriage on an air bearing further helps this. The critical features of the technique are the requirement of a long precision glass V-groove to hold the fiber in position with submicron accuracy, high beam quality of the pulsed laser, an accurate control system for fiber translation, and above all, stability of the pulsed source for imprinting gratings of a well-determined index of modulation. Since the fabrication process imprints overlapping gratings, it is possible to change the period or the modulation index locally or continuously along the length of the grating. A detail of the printing process is shown in Fig. 3.22. This system is flexible and is able to cater for any type of grating, including those with phase steps, chirp, apodization (see Section 3.1.9 and Chapter 5).

A slight modification of the MPF scheme is shown in Fig. 3.23. Here not only the fiber is allowed to move, but also the interferometer [49]. In this case, the interferometer is the phase mask that moves at a velocity

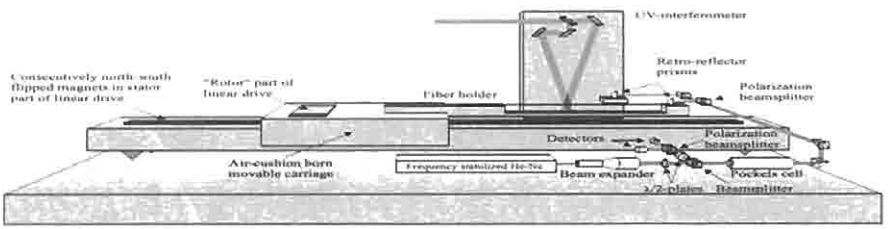

Figure 3.21: The multiple printing in fiber (MPF) grating technique. The substantial carriage is potentially capable of movements of up to 1 meter (courtesy R. Stubbe).

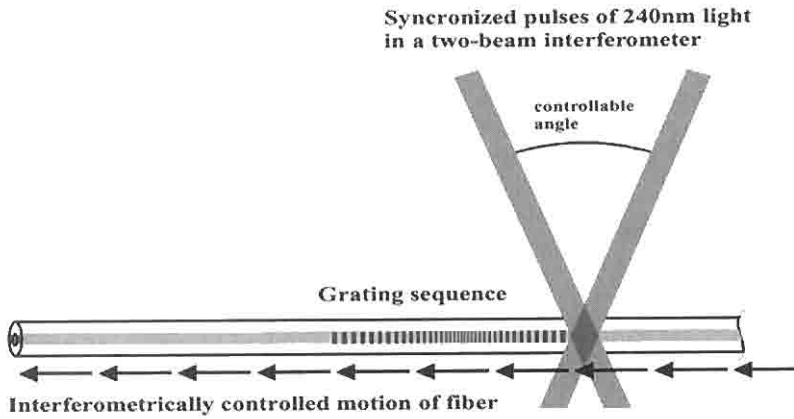

Figure 3.22: A detail of the MPF technique showing the imprinting of a mini overlapping grating to produce the required profile or chirp; the movement of the fiber is interferometrically controlled, and the imprinting is synchronized with the arrival of the UV pulses (courtesy R. Stubbe).

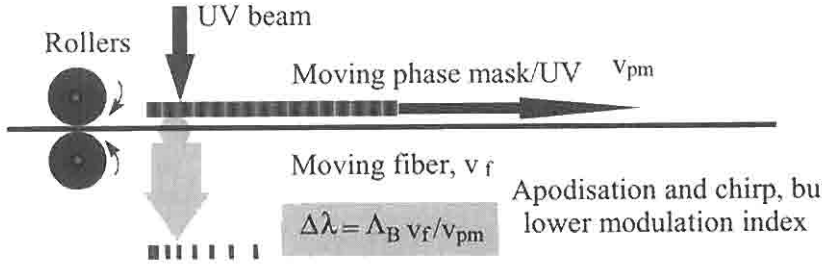

Figure 3.23: A technique based on the moving phase mask and fiber. If the phase mask is not moved, it is identical to the MPF method, but can only be used to write unchirped gratings using a pulsed source.

of v_{pm}, while the fiber moves with a velocity v_f. The change $\Delta\lambda$ in the period Λ_g of the grating is a function of the relative velocities, as

$$\Delta\lambda = \Lambda_{Bragg} \frac{v_f}{v_{pm}}. \tag{3.1.11}$$

Thus, a chirp may be programmed in the control computer by altering the relative velocities locally. A limitation is the need for a small spot size if a large chirp is being imparted in the grating in a long fiber, since the

maximum change in the period is a single period over the length of the UV writing spot, as

$$\Delta\lambda = \frac{\Lambda_{Bragg}}{2w}, \tag{3.1.12}$$

where w is the radius of the spot used for writing the short section of grating. Combining Eqs. (3.1.11) and (3.1.12) gives the following interesting relationship:

$$2w = \frac{v_{pm}}{v_f}. \tag{3.1.13}$$

Equation (3.1.13) suggests the use of a minimum spot size related to the relative velocities. Further, it should be noted that at any one time, an entire grating of spot size $2w$ is written with a constant amplitude and period. In the limit, this method trades in some of the refractive index modulation for chirp, but can at best imprint a quasi-stepped function instead of a continuous one, especially when the grating is being apodized.

3.1.13 Tuning of the Bragg wavelength, moiré, Fabry–Perot, and superstructure gratings

The effective index of a propagating mode in a fiber is both temperature and strain sensitive. The functional dependence of the mode index is given by the relationship

$$\partial n_{eff} = \frac{\partial n_{neff}}{\partial T}\Delta T + \frac{\partial n_{neff}}{\partial \sigma}\Delta\sigma, \tag{3.1.14}$$

where $\partial n/\partial T$ is the temperature coefficient of refractive index, ΔT is the change in temperature, $\partial n/\partial\sigma$ is the longitudinal stress optic coefficient, and $\Delta\sigma$ is the applied longitudinal stress. Since the Bragg wavelength is a function of n_{eff} [see Eq. (3.1.4)], the simplest method of altering the transfer characteristics of a fiber grating is to impose a temperature or strain profile along the length of the grating. However, prestraining a fiber during grating fabrication alters the Bragg grating wavelength in the relaxed state [7]. It is also possible to multiplex several gratings at the same location to form moiré type gratings [7,77]. It should be noted that the Bragg wavelengths of all multiplexed gratings written at the same location shift to longer wavelengths as each grating is superimposed.

The shift in the wavelength of the gratings is dependent on the *overall* change in the index of modulation, resulting in a change in the period averaged n_{eff} of the mode in the fiber. The *shift* $\Delta\lambda_{Bragg}$ in the Bragg wavelength, λ_{Bragg} as the UV induce index change δn increases can be shown to be

$$\Delta\lambda_{Bragg} = \lambda_{Bragg} \frac{\eta \delta n}{n_{eff}}, \tag{3.1.15}$$

where $\eta < 1$, is the overlap of the guided mode and the distribution of the refractive index modulation (see Chapter 4). Thus, when a grating is superimposed on an already-written grating, both gratings move to longer Bragg wavelengths.

By altering the angle of the interfering beams, several gratings may be written at a single location using the prism interferometer or the Lloyd mirror arrangement discussed in Section 3.1.6. These gratings show interesting narrow band-pass features with uniform period [77] or chirped gratings [78], and are discussed in Chapter 6.

If the temperature distribution along the length of a uniform grating is a linear function of length, then the Bragg wavelength, too, will vary linearly with length. The grating will demonstrate a linear chirp. This means that the different wavelengths within the bandwidth of the grating will not be reflected from the same physical location and the grating will behave as a dispersive component. The temperature profile (or the strain profile) may be altered to change the functional property of the grating [79]. On the other hand, prestraining or imposing a temperature profile along a fiber prior to writing a fiber grating will also result in a chirped fiber grating once it is written and the stress/temperature profile is removed [80,81]. However, the chirp in a grating fabricated in such a way will have the opposite sign of a grating chirped by the application of a temperature or strain profile after it has been manufactured.

During fabrication of the grating at an elevated temperature T_w, the Bragg wavelength will be defined by the period, Λ_g of the grating. After fabrication, when the temperature is returned to a final temperature T_f, the Bragg wavelength will be

$$\lambda_{Bragg} = 2\Lambda_g(1 + \alpha[T_f - T_w])\left(n_{eff} + \frac{dn_{eff}}{dT}\left[T_f - T_w\right]\right), \tag{3.1.16}$$

where α is the thermal expansion coefficient of the fiber and dn_{eff}/dT is the temperature coefficient of the mode index; to the first approximation,

this is merely the change in the refractive index of the fiber core as a function of temperature. Equation (3.1.16) may be simplified by expanding and rearranging to

$$\lambda_{Bragg} = 2\Lambda_g\left\{n_{eff}[1 + \alpha(T_f - T_w)] + \frac{dn_{eff}}{dT}(T_f - T_w)\right\}. \quad (3.1.17)$$

The thermal expansion coefficient of silica α is approximately $+5.2 \times 10^{-7}$, whereas $dn/dT \approx +1.1 \times 10^{-5}$ °C^{-1}; the contribution of the thermal expansion coefficient term is approximately 10% in comparison. Equation (3.1.17) is further simplified to

$$\lambda_{Bragg} \approx 2\Lambda_g\left\{n_{eff} + \frac{dn'}{dT}(T_f - T_w)\right\}, \quad (3.1.18)$$

where the combined effect of the thermal expansion and the refractive index change is included in n', so that the change shift in the Bragg wavelength is simply

$$\Lambda\lambda_{Bragg} \approx 2\Lambda_g \frac{dn'}{dT}(T_f - T_w). \quad (3.1.19)$$

Typically, $dn'/dT \approx 0.5$ to 1.0×10^{-2} °C^{-1}. At a wavelength of 1500 nm the change in the Bragg wavelength with temperature is ~1 to 2×10^{-2} nm °C^{-1} [82,7].

With long uniform gratings, a thin heating wire suitably placed below a point in the grating can result in a distributed feedback (DFB) structure, with a double-peaked reflection spectrum. The transfer characteristics of each half of the grating are identical; however, a $\lambda/4$ phase difference induced by the heating wire causes a hole to appear within the band stop [83]. Such a grating in rare-earth-doped fiber can be used in DFB lasers, which require the suppression of one of the two lasing modes to force the laser into single-frequency operation, and in narrow band-pass filters. A number of methods have been reported for fabricating DFB structures in fibers, including postprocessing a uniform grating to locally induce a "gap" in the center of the grating [84]. Alternatively, two gratings may be written on top of each other, each with a slightly shifted wavelength to form a Moiré phase-shifted grating, opening a bandgap once again [77].

Radic and Agrawal [85] reported that using an additional quarter-wave phase shift within a grating opens up yet another gap. An extension of this principle directly leads to the superstructure grating, which has been extensively used in tunable semiconductor-laser design [86]. A schematic of the superstructure grating is shown in Fig. 3.24. The composite grating consists of a number of subgratings of length ΔL (but not necessarily of identical lengths), which are separated by "dead" zones of length δl (these lengths may be different). The superstructure grating was first demonstrated in an optical fiber by Eggleton *et al.* [87], produced by a phase mask. A more general problem of stitching errors in phase masks has been addressed by Ouellette *et al.* [88]. Multiple reflections occur within the bandwidth of a single subgrating; each reflection has a bandwidth defined by the length of the grating without the gaps, i.e., $N\Delta L = L_g - (N-1)\delta l$.

The Fourier components of the grating shown in Fig. 3.24 basically have a fundamental component with a uniform period Λ_g and a fundamental modulation envelope of period $\Lambda_e = \delta l + \Delta L$. Thus, the reflection spectrum will have components at the sum and difference frequencies. The new reflection wavelengths, λ^{-}_{Bragg} and λ^{+}_{Bragg}, are calculated from Eq. (3.1.4):

$$\frac{1}{\lambda^{-}_{Bragg}} = \frac{1}{2n_{av}\Lambda_g} + \frac{1}{2n_{av}\Lambda_e} \tag{3.1.20}$$

and

$$\frac{1}{\lambda^{+}_{Bragg}} = \frac{1}{2n_{av}\Lambda_g} - \frac{1}{2n_{av}\Lambda_e}, \tag{3.1.21}$$

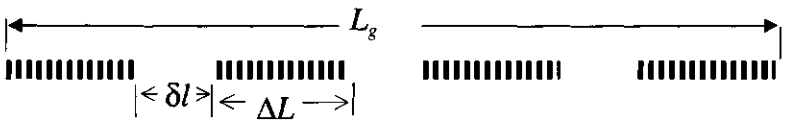

Figure 3.24: A schematic of a superstructure grating. This is constructed by blanking $(N-1)$ sections of length δl in a long continuous grating of length L_g. The superstructure grating is a collection of cascaded Fabry–Perot interferometers.

where n_{av} is the average index of the mode. It follows, therefore, from Eqs. (3.1.20) and (3.1.21) that the new grating periods Λ_g^- and Λ_g^+ corresponding to the superscripted Bragg wavelengths are

$$\Lambda_g^- \approx \Lambda_g\left(1 - \frac{\Lambda_g}{\Lambda_e}\right)$$
$$\Lambda_g^+ \approx \Lambda_g\left(1 + \frac{\Lambda_g}{\Lambda_e}\right). \tag{3.1.22}$$

From Eqs. (3.1.4) and (3.1.22), it follows that the spacing $\Delta\lambda$ between the reflected wavelengths in any such superstructure is

$$\Lambda\lambda = 2n_{av}\frac{\Lambda_g^2}{\Lambda_e}. \tag{3.1.23}$$

Depending on the shape of the composite structure (and thus the magnitudes of the individual Fourier components), higher order components can appear [87].

Superstructure gratings represent a number of types of gratings: the DFB with a single phase step $\phi < 2\pi$ [85,86]; the grating Fabry–Perot with $\phi \gg 2\pi$ resulting in multiple high-finesse transmission peaks [89]; cascaded grating Fabry–Perots in which the phase steps $\phi \gg 2\pi$ [87], leading to replicated multi-band-pass transmission spectra; gratings with multiple-flat-top reflection spectra, fabricated with unequal grating lengths as well as phase steps [90]; and truly flat-top reflection gratings fabricated by introducing regular $\pi/2$ phase shifts ($\lambda/4$) at equal intervals, while altering the strength of the grating amplitude in each section to mimic a *sinc* function [91].

There are several methods of making these gratings. In order to introduce a specific phase step, the simplest and most reliable is via the replication of a phase mask with the appropriately prerecorded phase steps [92]. Another method successfully used for introducing a $\pi/2$ phase step in a grating is by UV postprocessing [84]. After the grating has been written, the small central section is illuminated with UV radiation to introduce a phase shift. As the refractive index of the exposed region of length δl increases by δn, the transmission spectrum of the grating is monitored to stop the exposure when $\delta n \delta l = \lambda/4$. A disadvantage of post-UV exposure is that it not only changes the phase between the two halves of the grating, but also alters the local n_{eff} of the fiber. This in turn shifts the Bragg wavelength of the already-written grating exposed to UV

radiation to a longer wavelength. The effect of the shift is a slightly broader overall reflection spectrum.

The use of an amplitude mask in conjunction with a phase mask allows the precise printing of a superstructure grating [93]. Of course, mini-gratings may be printed by precise translation of the fiber between imprints [91,73]. This method has been used to write a *sinc* function grating with remarkably good results. However, it is difficult to write a continuous *sinc* function. Approximating the *sinc* function in a limited number of steps creates additional side bands, which limits the out-of-band rejection in the reflection spectrum. Combing the *sinc* function grating with apodization results in an improved transfer function, increasing the depth of the out-of-band rejection [91].

Chirped gratings are useful for many applications. There are a number of ways of chirping gratings, including writing a uniform period grating in a tapered fiber [94], by application of varying strain after fabrication [43,79,95], by straining a taper-etched fiber, by fabrication by a step-chirped [96] or continuously chirped phase mask, or by using one of the several schemes of writing a cascade of short, varying-period gratings to build a composite, long grating. These methods for writing chirped gratings are discussed in Section 3.1.14.

The properties of many of these gratings along with their applications may be found in Chapter 6.

3.1.14 Fabrication of continuously chirped gratings

Short, continuously chirped gratings are relatively straightforward to fabricate; longer (>50 mm) ones become more difficult. One of the simplest methods is to bend a fiber such that a continuously changing period is projected on it. This is shown in Figure 3.25 in which the fiber is bent either in the fringe plane or orthogonal to it. Altering the lay of the fiber may change the functional dependence of the period on position, so that either linear or quadratic chirp may be imparted.

Figure 3.26 shows a curved fiber with a radius of curvature R in a fringe plane. At any point of arc a distance S from the origin O where the fiber axis is normal to the fringe planes, the local period of the grating can be shown to be

$$\Lambda_s = \frac{\Lambda_g}{\cos(S/R)}, \tag{3.1.24}$$

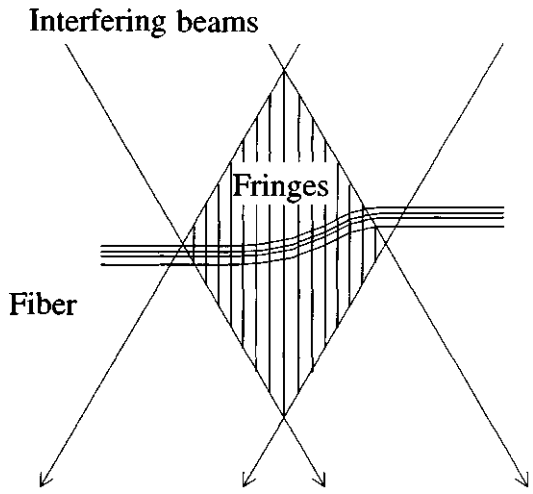

Figure 3.25: Writing of a continuously chirped grating by bending the fiber in the fringe plane. Note that the bending also causes the grating to be blazed with respect to the fiber axis.

so that even with a large radius of curvature, the grating may be substantially chirped. Gratings with bandwidths of 7.5 nm and peak reflectivity of 99%, as well as 15-nm bandwidth with a peak reflectivity of 5%, have been reported with this technique [98].

As in the case of fiber tilted with respect to the fringe planes, bending has a similar effect of imparting a blaze and consequently radiation loss. The loss, which manifests itself on the short-wavelength side of the Bragg wavelength even in unblazed gratings, is increased by blazing and may not be desirable; for a chirped grating, this can be a serious problem, if the radiation loss spectrum lies within the chirped bandwidth of the grating. Loss due to coupling to cladding modes in chirped gratings can be reduced by using fibers that are strongly guiding, but cannot be entirely eliminated. It may be substantially reduced, however by the use of special fibers with a photosensitive cladding [97] (see Chapter 4).

A constant strain along the length of a fiber while a grating is imprinted merely shifts the Bragg wavelength on strain release. In order to impart a chirp, a nonuniform strain profile has to be used, and there are several practical methods for implementing this. If an optical fiber is tapered (e.g., by etching) such that the outer diameter varies smoothly in the region of grating, the application of a longitudinal force leads directly to strain that

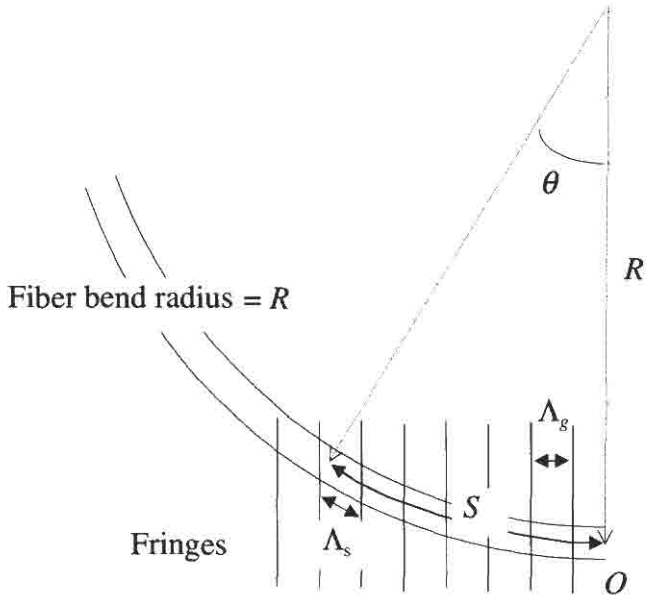

Figure 3.26: A fiber curved with a radius R in the fringe plane. The period of the grating seen by the fiber varies continuously along its length S.

is nonuniformly distributed along its length. The local strain ε_l may be computed from the local cross-sectional area A_i as [80]

$$\varepsilon_i = \varepsilon_{i-1} \frac{A_{i-1}}{A_i}, \tag{3.1.25}$$

where the subscript $(i - 1)$ refers to the previous section of the grating. Thus, a linear change in the cross-sectional area leads to a linear chirp. Applying positive strain to a uniform-period grating in a tapered fiber has three effects: the mean Bragg wavelength of the entire grating shifts to *longer* wavelengths, and the grating reflection spectrum broadens, while being reduced in reflectivity. Alternatively, the tapered fiber may be strained before writing of the grating. On strain release, the grating becomes chirped, but now shifts to a *shorter* wavelength. If a chirped grating is written in a strained tapered fiber such that the longer wavelength is inscribed in the narrower diameter, releasing the strain has the

effect of *unchirping* the grating. If the relieved strain is too large, the grating becomes chirped once again but with an *opposite* sign of chirp: i.e., the narrower diameter end has a shorter wavelength than the larger diameter end. The method is capable of high reproducibility, is simple to implement, and allows nonlinear chirps to be programmed into the grating [80]. There are two factors that affect the Bragg wavelength in strained etched fibers: the change in the physical length of the fiber, and the effective index of the mode through the stress-optic effect,

$$\Lambda\lambda|_{\sigma=0} = 2\Lambda_g \partial n_{eff} + 2n_{eff}\Lambda_g \varepsilon_i, \tag{3.1.26}$$

where the change in the Bragg wavelength is $\Delta\lambda$ under zero stress, *after* the grating has been written under local strain of ε_i, and δn_{eff} is the change in the effective index of the mode due to the strain-optic coefficient. The two quantities on the RHS in Eq. (3.1.26) have opposite signs, with the strain term being much larger than the stress-optic coefficient. Nevertheless, when a grating is written in a tapered fiber under strain, it appears chirped, although the period of the grating is uniform. Because of the stress-optic effect, the local effective index of the mode is not uniform along the length of the grating. On removal of the strain after the grating has been inscribed, the effective index of the mode becomes uniform, but the period is altered because of the change in local strain, and the grating becomes uniform at some lower strain value and chirped with the opposite sign when fully relaxed.

Etched linear tapers produce nonlinear chirp, since the chirp is inversely proportional to the square of the radius of the section according to Eq. (3.1.25). Since the Bragg wavelength is directly proportional to the applied strain [see Eq. (3.1.14)], the induced chirp becomes nonlinear. To compensate for this disparity, a nonlinear etching profile [99] can be used, resulting in a linear chirp. In order to fabricate a predetermined etch profile, the time of immersion of the fiber in the etching solution (usually buffered hydrofluoric acid) must be controlled, since the etch rate at constant temperature is highly reproducible. A three-section vessel with a layer A of a mixture of decahydronaphthalene and dichlorotoluene (10%) floating above layer B of 32% HF and with a third layer C of trichloroethylene below it may be used. This allows the acid to come into contact only with a small section of the fiber when it is immersed vertically into it. With the fiber remaining in position, the vessel is lowered at a programmed rate to expose another part of the fiber in section B, while the top layer A immediately stops the fiber from etching any further. Using this method, highly repeatable tapers have been produced and linear chirps of 4.8 nm

demonstrated [100]. Using the same method, different structures have been fabricated, such as a grating with a $\pi/2$ phase shift in the middle. A fiber in which the taper in one half has been etched more than the other was stretched before a grating was written. Relaxing the fiber introduced a phase shift and therefore a band pass in the center of the transmission spectrum of the otherwise unchirped grating [99].

A somewhat less flexible method relies on the tapering of the fiber core [94]. Tapering the core affects the local effective index n_{eff} of the mode. To the first approximation, the effective index varies linearly with decreasing diameter for an initial fiber V-value of approximately 2.4, but varies more slowly, asymptotically approaching the cladding index, as the core diameter goes to zero. Thus, a uniform-period grating written in tapered section will be chirped. The *maximum* chirp $\Delta\lambda$ achievable in a fiber may be calculated from

$$\Delta\lambda \approx \lambda_{Bragg} \frac{\Delta n}{n_{eff}}, \tag{3.1.27}$$

where Δn is the difference between the mode index and the cladding refractive index, Equation (3.1.27) translates to a maximum chirp on the order of 30 nm ($\Delta n = 0.03$); however, it would be difficult for practical reasons to achieve more than ~10 nm of chirp.

A chirp of 2.7 nm for a 10-mm long grating was reported for a fiber tapered by 50 μm over that length [94]. Local heating and stretching may fabricate a tapered fiber. Note, however, that a fiber with a large taper will have a lower reflectivity for the shorter wavelengths (with a uniform period grating), since the mode power spreads to the nonphotosensitive cladding, reducing the efficiency of the grating.

Another technique, that overcomes the problem associated with the core-taper method described above is based on expanding the core by thermal out-diffusion of the photosensitive core dopant [101]. The important difference between the two methods is that while the tapering of the core *reduces* the V-value of the fiber, the out-diffusion of the photosensitive core leaves the V-value *unchanged* [102]. This may be understood by remembering that the reduction in the core index as the dopant out-diffuses is compensated for by the increase in the core radius. The fractional power in the core remains unchanged (due to the fixed V-value), but since the core index is reduced, so is the mode index.

Heating the fiber locally by an oxyhydrogen flame for 2 minutes resulted in the mode field diameter expanding from 7.8 to 16.8 μm. Subsequent writing of a 10-mm long grating in the tapered core region of a

hydrogenated sample resulted in a chirped grating with a bandwidth of 6.0 nm [101].

Stretching a fiber prior to writing a grating shifts the Bragg wavelength in the relaxed state [7]. Byron and Rourke [103] applied the stretch–write technique to form a chirped grating with a scanned phase mask. As the UV beam (2 mm long) was stepped across the phase mask (and the fiber), the prestrained (0.6%) fiber was also relieved of strain in 15 steps of 0.04%. A chirped grating with a bandwidth of 10 nm for a grating length of 30 mm was demonstrated. Care has to be taken with this method, since the fiber can easily slip when under tension.

As will be appreciated with the above methods, the bandwidth of the chirp is generally small; in order to increase the chirp, it is necessary to write a chirped grating in the first place. Continuously chirped gratings with larger chirp values can be fabricated with two beams with dissimilar phase fronts. If one parallel beam is interfered with a second diverging beam, the resulting interference pattern will have a period that varies with spatial position in the fringe plane. Figure 3.27 shows the scheme for writing chirped gratings with two diverging, two converging, or a

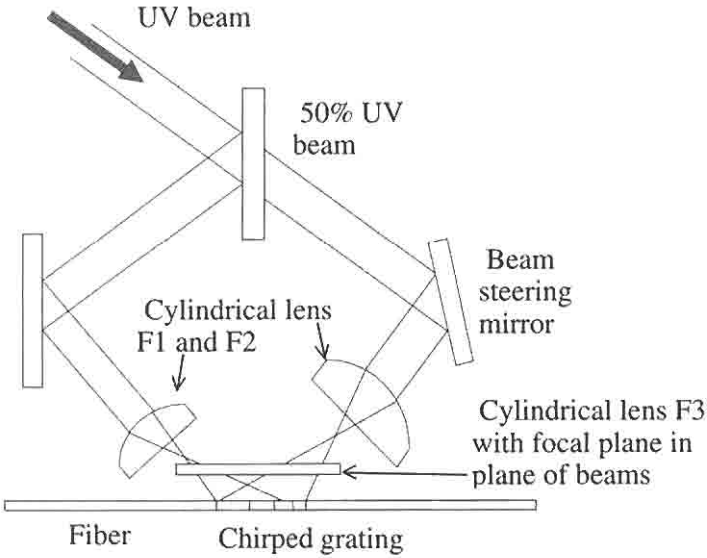

Figure 3.27: Nonuniform wave fronts used in the interferometer to produce chirped gratings [104]. Two cylindrical lenses with focal lengths F1 and F2 create a chirped interference pattern at the fiber. The third cylindrical lens with focal length F3 focuses the interfering beams into a stripe at the fiber.

combination of interfering beams. The advantage of using lenses as chirp-adjusting elements is that any chirp bandwidth is possible, limited only by the photosensitive response of the fiber. Using such an interferometer, chirp bandwidths of 44 nm have been demonstrated with a reflectivity of ~80%, covering the entire erbium amplifier gain band. The mechanical and geometrical positioning of the lenses makes the interferometer easy to use, although the repeatability may be not be so good. A disadvantage of this method is the strong curvature of the fringe pattern inscribed in the fiber, which results in coupling of light to the radiation modes on the blue side of the grating transmission spectrum [104].

3.1.15 Fabrication of step-chirped gratings

Gratings that are chirped in discrete steps are known as step-chirped. The concept was introduced by the fabrication of phase masks, which were not continuously chirped [23]. Figure 3.28 shows the principle of this type of grating. The grating of length L_g is split into N sections, each of length δl and uniform period Λ_n ($1 < n < N$), differing from the previous one by $\delta\Lambda$, with

$$\delta\Lambda = \frac{\Delta\Lambda_g \delta l}{L}, \tag{3.1.28}$$

where $\Delta\Lambda_g$ is the total chirp of the grating and $L_g = \delta l \times N$. If the change in the period and the sections are sufficiently small, then the grating becomes continuously chirped. The important choice is the number of sections required to build in the chirp. This has been analyzed [105], and it was shown that the length δl of the uniform period section should be

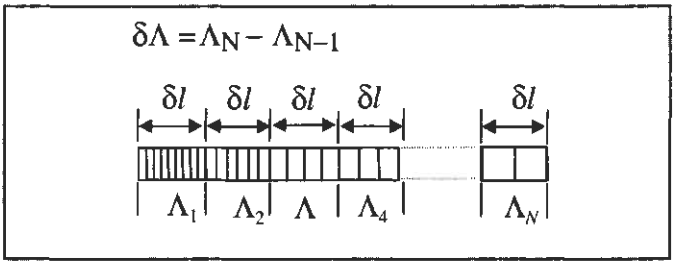

Figure 3.28: The step-chirped phase mask. It is important to ensure that each section of the grating has an integral number of grating periods, so that the section lengths δl are only nominally identical [23].

such that its bandwidth is ~50% greater than the chirp $\Delta\Lambda_g$ of the grating, irrespective of length of the grating. Making this choice results in a deviation of the characteristics of the grating that differ <1% from those of a continuously chirped grating. There must be an integer number of periods in each subsection to ensure that phase mismatch does not occur. A result of this requirement is that the lengths of the subsections are only approximately equal.

The step-chirped grating is ideally implemented in the phase mask using e-beam lithography [23]. Splitting a grating into small fields is exactly how the e-beam process works [20], so that it is naturally suited to the fabrication of step-chirped phase masks. Wide and narrow bandwidth (1–50 nm) phase masks have been fabricated with linear and quadratic step chirps [23] and used for pulse recompression of femtosecond pulses transmitted over optical fiber [106]. Step-chirped phase masks 100 mm long, useful for dispersion compensation in telecommunications transmission links [107], have also been demonstrated [108,74].

There are other techniques that mimic the step-chirped gratings, for example, with a limited chirp capability, using stretch and write [103] discussed in Section 3.1.14. Riant and Sansonetti have also shown that by the use of a focusing lens and a phase mask, small sections with different wavelengths can be built up to create a step-chirped grating [109]. Focusing or defocusing a beam at a phase mask changes the wavelength of the inscribed period in the fiber immediately behind the phase mask. Thus, stepping the spot along the mask while adjusting the focus allows the inscribed wavelength to be altered at each step. Using this method, 50-mm long gratings have been demonstrated with chirp values of ~1 nm [109].

There is great advantage in the use of the step-chirped phase-mask, since it allows not only the definition of the grating wavelength, but also any value of chirp rate. The minimum chirp bandwidth possible is, of course, limited by the natural bandwidth of a grating of length L_g.

An extension of the step-chirped principle is the concept of super-step-chirped gratings [75]. This technique allows even longer gratings to be assembled using a set of short step-chirped phase masks. This overcomes a major limitation of e-beam fabrication: the writing of masks longer than 100 mm is difficult and expensive. An alternative is to fabricate several gratings on a single-phase mask plate, each with a fixed chirp. Each phase mask is designed to begin at a wavelength $\delta\lambda$ longer than the wavelength at which the last phase mask finished. The gratings on the phase mask are aligned one above the other with exactly the

correct lengths. After a single grating is scanned into the fiber, the fiber is translated along accurately, and the next phase mask grating moved vertically into position for writing the succeeding grating. Any small inaccuracy in the placement (stitching) of the phase mask grating can be "trimmed" [110], using a single UV beam exposure to adjust the phase between adjacent sections [112].

Using this method, gratings 2 *meters* long have been written in a single contiguous piece of fiber, with a chirp bandwidth of ~15 nm [111], and a 1.3-*meter* long grating with a bandwidth of 10 nm has been used for multichannel dispersion compensation [75,112].

The detailed characteristics of step-chirped and super-step-chirped gratings are discussed in Chapter 4.

3.2 Type II gratings

Fiber gratings formed at low intensities are generally referred to as Type I. Another type of grating is a damage grating formed when the energy of the writing beam is increased above approximately 30 mJ [119]. Physical damage is caused in the fiber core on the side of the writing beams. The definite threshold is accompanied by a large change in the refractive index modulation. It is therefore possible to write high-reflectivity gratings with a single laser pulse. Above 40–60 mJ, the refractive index modulation saturates at around 3×10^{-3}. Energy of the order of 50–60 mJ can destroy the optical fiber. The sudden growth of the refractive index is accompanied by a large short-wavelength loss due to the coupling of the guided mode to the radiation field. The gratings generally tend to have an irregular reflection spectrum due to "hot spots" in the laser beam profile. By spatially filtering the beams, gratings with better reflection profiles have been generated but with a much reduced reflectivity [113]. These gratings decay at much higher temperatures than Type I, being stable up to ~700°C. Some of the properties of these gratings are outlined in Chapter 9.

3.3 Type IIA gratings

Yet another type of grating is formed in *non*-hydrogen-loaded fibers. These may form at low power densities or with pulsed lasers after long exposure [114]. The characteristics of a Type IIA grating are the growth of a zero-order ($N = 1$) grating, and its erasure during which a second-order grating

grows at approximately half the initial Bragg wavelength, followed by the growth of the $N = 1$ grating. The final grating is stronger than the original and is able to withstand a higher temperature. These gratings form in most fibers, although they have yet to be observed in hydrogen-loaded fibers. The gratings are reviewed in Chapters 2 and 9.

3.4 Sources for holographic writing of gratings

There are several UV laser sources that may be used for inducing refractive index changes and for fabricating gratings in optical fibers. Methods for generating UV or deep UV radiation require the use of excimer lasers, nonlinear crystals for frequency mixing of coherent visible/infrared radiation, or line-narrowed dye laser radiation. UV laser sources may be categorized into two types — low spatial/temporal coherence or spatially coherent sources. Sources in the first category have been used extensively for grating fabrication but need to be used with care for high-quality grating production. The primary advantage is in the high average and peak power available in the UV region. On the other hand, some frequency mixing methods produce UV radiation of high temporal and spatial coherence and are ideally suited for grating formation. Typically, these lasers demonstrate high average power capability but have the disadvantage of lower peak power densities. Nevertheless, these have also been shown to be highly successful for inducing large index changes while maintaining excellent grating quality.

3.4.1 Low coherence sources

The first source reported for use in grating formation was the excimer-laser pumped frequency doubled oscillator–amplifier dye laser operating in the 240-nm window [13]. This source can produce approximately 0.1 W average tunable radiation between 240 and 260 nm using a β-barium borate (BBO) crystal by doubling the (CHRYSL 106) dye-laser output. The laser must be line-narrowed to increase the coherence length, and longitudinal pumped dye lasers are preferable since they produce a higher quality beam compared to side-pumped dyes which produce a triangular beam profile. An alternative pump laser for the dye is the frequency-mixed output at 355 nm from a YAG laser operating at a wavelength of 1064 nm. Similar output may be achieved with a maximum of around

120 mW average at 244 nm for a 20-Hz system with 12-ns pulses [115]. The frequency-doubled tunable dye-laser source can be line-narrowed to increase temporal coherence, helping maintain interference despite path-length differences. However, the UV beam may need to be spatially filtered if the beam-quality is not good so as to be able to write uniform reflection gratings. High-quality gratings have been reported using this method [116], however, by multiple pulse writing.

With low transverse coherence, it is still possible to write good gratings, provided the spatial nonuniformity averages out over the time period required to write the grating. However, the pulse-to-pulse transverse beam variation affects single-pulse writing of gratings [117–121] or, for example, during fiber drawings [122,123], as was originally suggested by Askins *et al.* [118]. The power density variation manifests itself in two ways: first, the reflectivity varies from grating to grating, and second, the peak reflection wavelength, which is a function of the induced index change, varies between gratings. Beam profile nonuniformity has a rather more serious deleterious effect on the grating reflection spectrum, causing multiple peaks and chirp. The spectral shape is discussed in more detail in Chapters 4 and 9. Multiple pulses can ensure that each section of the grating can be driven into saturation (for a given UV flux), although if the beam profile has a Gaussian average intensity profile, the grating will appear chirped. The regions with low flux will see a smaller index change and hence a smaller change in the effective index of the mode than the central region of the beam. Since the Bragg wavelength is proportional to the effective index of the mode, the beam profile imparts a Bragg wavelength profile proportional to the intensity profile, leading to chirp [124]. It is for this reason that there is a concern over the use of a laser with "hot-spots" in the beam. The grating may show *fine* structure in the reflection spectrum due to the nonuniform refractive index modulation of the inscribed grating. This has so far not been reported in the literature but may well be a problem for long gratings.

Another aspect of low coherence sources, which must be taken into account when designing an interferometer, is the effect of the coherence length. These laser sources are generally better suited to direct printing using a phase mask with the fiber immediately behind the phase plate. Alternatively, a one-to-one imaging system may be used to form the interferometer such that the path of the two beams are equalized and overlapped. If, however, the paths are not equal or the beams do not overlap, degradation in the visibility can result in poor grating reflectivity and/or spectral profile. The limiting factor for all lasers is the divergence of the

beam, which determines how far away the fiber may be placed from the phase mask as (see Fig. 3.1)

$$\delta\lambda \, \delta\phi \ll \lambda^2 \frac{\cos(\theta_m/2)}{2L}, \tag{3.4.1}$$

where $\delta\lambda$ is the source bandwidth, $\delta\phi$ the source angular divergence, λ the source wavelength, $\theta_m/2$ the half diffraction angle, and L the distance of the fiber from the phase mask. The physical significance of Eq. (3.4.1) is that as the diffracted beams are brought together, the divergence causes a dephasing of the interfering beams, reducing the visibility. The contact method is therefore ideally suited for use with low-coherence sources. However, it must be remembered that the phase mask is more likely to be damaged owing to contamination from the fiber, i.e., dust, etc., using high-intensity pulses.

High peak-power laser sources do allow the writing of Type II gratings, which depend on physical damage to the core region [125]. This aspect is discussed in Section 3.2.

3.4.2 High coherence sources

Lasers with good spatial and/or temporal coherence fall in this category. Examples include CW intracavity frequency doubled argon-ion lasers operating at 257 nm/244 nm [26,126], QS frequency quadrupled YLF [127], spatially filtered, line-narrowed frequency doubled dye lasers [13]. The first laser has excellent spatial and temporal coherence, being derived from the argon ion laser mode. Even with this laser, there can be fine structure in the transverse beam profile of the UV mode due to the low walk-off angle in the frequency doubling crystal, BBO. The beam is elliptical, but this is an advantage because the shape is suited to writing fiber gratings. The latter two lasers can be made to have good temporal coherence by line narrowing, but requires good spatial filtering to generate a satisfactory Gaussian mode profile. The pinholes used for filtering require careful alignment and have a tendency to burn after a short time owing to the high peak power; they require frequent replacement.

The quadrupled Nd:YLF and the intracavity frequency doubled argon ion lasers belong to the class of turnkey systems. These are reliable lasers and need little attention other than routine maintenance; for example, mirrors need occasional cleaning. The frequency doubling crystals tend to be KTP for the YLF followed by a BBO crystal enclosed in an airtight holder with silica windows. Although the transverse mode profile may

not be uniform shot-to-shot for this laser, it does allow the use of cylindrical lenses for focusing into the BBO crystal. This scheme overcomes the transverse walk-off problem in BBO associated with spherical lens focusing. However, it is not possible to use cylindrical focusing in the intracavity frequency doubling in BBO. A schematic of the Z-folded resonator is shown in Fig. 3.29. With careful adjustment of the fold and focusing mirrors, this laser can be operated at a stable CW output in excess of 300 mW at 244 nm. A cylindrical lens can be used at the output to circularize the beam. Typically, the beam diameter is approximately 2 mm.

The coherence length of the argon-ion laser operating in the single-frequency mode is more than adequate for use in a beam splitting interferometer even with path length differences approaching several centimeters, although the path length difference is usually not so large. This laser is also suited for use in the scanned phase-mask interferometer, or for writing blazed gratings, as discussed in Section 3.1.4.

Recent work on writing grating with near-UV wavelength radiation [128–130] means that other high-quality laser sources may be used for grating fabrication. An argon laser operating at 302 nm is one option, which allows the inscription of gratings directly through the silicone resin polymer jacket [71] or the use of a novel polymer at a wavelength of 257 nm [70]. The lifetime of the argon ion laser operating in the UV is probably an issue for the fabricator. However, other sources as yet not demonstrated, e.g., the intracavity krypton ion laser operating at 647 nm, frequency doubled to 323.5 nm, would be an attractive option, with plenty of power available at the UV wavelength.

3.1 lists a summary of the different types of lasers operating in the UV, used for grating fabrication.

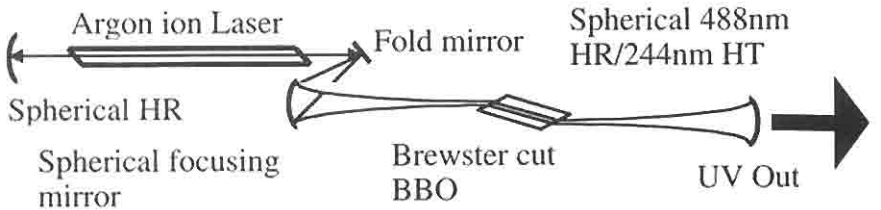

Figure 3.29: A schematic of the intracavity frequency-doubled, argon ion laser. 488-nm wavelength radiation is doubled to generate 244-nm UV emission. Angle tuning does phase matching of the BBO crystal. It is not necessary to temperature stabilize the BBO crystal [26].

Table 3.1: Common options of UV laser sources for grating formation.

Pump laser	UV wavelength (nm)	UV power/energy	Beam shape	Beam quality	Application
KrF	248	1 J/100Hz, QS	Few cm diameter	Low spatial/ temporal coherence: requires injection locking	Mass production, fiber drawing tower grating fabrication, TYPE II gratings
ArF	193	1 J(100Hz) QS	Few cm diameter	Low spatial/ temporal coherence	Planar devices, non-Ge fibers/planar, direct writing
Quadrupled Nd:YAG (1064 nm)	266, KDP/BBO frequency doublers	>100 mW 5 ns QS pulses at >1kHz	1 mm diameter	10 mm coherence length, low transverse beam coherence	Hydrogen loaded fibers, planar Ge/P doped silica, + RE-doped silica, Type II gratings
Nd:YAG (355 nm via frequency mixing)	220–260 tunable extra cavity BBO frequency doubled	>100 mW, 4 ns QS	2 mm diameter, not Gaussian, flat-topped or triangular	Low coherence, unless line-narrowed	UV-induced index change studies, grating writing, material studies, Type II grating formation, scanned phase mask

XeCl (308 nm) pumped dye laser	Same as above	Same as above	Same as above	Same as above	Same as above
Argon ion laser, 514/488 nm	257, 244, intracavity frequency-doubled in KDP/BBO	Up to ~2 W; up to ~1 W CW	1 mm, elliptical TEM00	High coherence, can be operated single-frequency but not necessary	Source with an excellent beam quality for grating fabrication; contact and noncontact phase mask/interferometer but not ideal for Type II gratings
Diode pumped quadrupled QS Nd:YLF (1048 nm)	262, frequency-doubled externally in KTP and BBO	~100 mW QS 100 ns pulses	~1 mm elliptical TEM00	Medium coherence, good beam quality	Good source for Type I and II grating writing in fibers and planar
Argon ion laser at 302 nm	Fundamental wavelength	~200 mW	1 mm TEM00	Excellent coherence: tube lifetime?	Writing through the jacket of D/H_2 loaded fibers
Krypton ion laser at 647 nm[a]	Frequency-doubled in BBO to 323.5 nm	>1 W	1 mm TEM00	Ideal near-UV source; long lifetime	Through the jacket inscription of D/H_2 loaded fibers

[a]Proposed by author; unused as yet.

References

1 Hill K. O., Fujii Y., Johnson D. C., and Kawasaki B. S., "Photosensitivity in optical waveguides: Application to reflection filter fabrication," *Appl. Phys. Lett.* **32**(10), 647 (1978).

2 Hill K. O., Malo B., Bilodeau F., and Johnson D. C., "Photosensitivity in optical fibers," *Ann. Rev. Mater. Sci.* **23**, 125–157 (1993).

3 Lam D. K. W. and Garside B. K., "Characterization of single-mode optical fiber filters," *Appl. Opts.* **20**(3), 440–445 (1981).

4 Lapiere J., Bures J., and Chevalier G., "Fiber-optic integrated interference filters," *Opt. Lett.* **7**(1), 37–39 (1982).

5 Kawasaki B. S., Hill K. O., Johnson D. C. and Fujii Y, "Narrow-band Bragg reflectors in optical fibers" *Opt. Lett.*, **3**(2), 66–68 (1978).

6 Bures J., Lapiere J., and Pascale D., "Photosensitivity effect in optical fibers: a model for the growth of an interference filter," *Appl. Phys. Lett.* **37**(10), 860 (1980).

7 Campbell R. J. and Kashyap R., "Spectral profile and multiplexing of Bragg gratings in photosensitive fiber," *Opt. Lett.* **16**(12), 898–900, (1991).

8 Stone J., "Photorefractivity in GeO_2-doped silica fibers," *J Appl Phys* **62**(11), 4371 (1987).

9 Hand D. P. and Russell P. St. J., "Single mode fibre gratings written into a Sagnac loop using photosensitive fibre: transmission filters," *IOOC, Technical Digest*, pp. 21C3–4, Japan (1989).

10 Bures J., Lacroix S., and Lapiere J., "Bragg reflector induced by photosensitivity in an optical fibre: model of growth and frequency response," *Appl. Opt.* **21**(19), 3052 (1982).

11 An Sungyuk and Sipe J. E., "The dynamics of phase grating formation in optical fibres," *SPIE* **1516**, International Workshop on Photoinduced Self-Organisation in Optical Fibre, Québec (1991).

12 Campbell R. J. and Kashyap R., "Properties and applications of photosensitive germanosilicate fibre," *International J. Optoelectron.* **9**(1), 33–57 (1994), and references therein.

13 Morey W. W., Meltz G., and Glenn W. H., "Holographically generated gratings in optical fibres," *Optics & Photonics News* **1**(7), 8 (1994).

14 Hill K. O., Malo B., Vineberg K. A., Bilodeau F., Johnson D. C., and Skinner I., "Efficient mode conversion in telecommunication fibre using externally written gratings," *Electron. Lett.* **26**(16), 1270 (1990).

15 Meltz G., Morey W. W., and Glenn W. H., "Formation of Bragg gratings in optical fibres by transverse holographic method," *Opt. Lett.* **14**(15), 823 (1989).

16 Lerner J. M., Flamand J., Laude J. P., Passereau G., and Thevenon A., "Diffraction gratings ruled and holographic — a review," in *Proc. of SPIE Symposium on Periodic Structures, Gratings, Moiré Patterns, and Diffraction Phenomenon,* vol. 240, pp. 82–88 (1980).

17 Okai M., Tsui S., Chinone N., and Harada, "Novel method to fabricate corrugations for a $\lambda/4$ shifted distributed feedback laser using a grating photomask," *Appl. Phys. Lett.* **55**, 415–416 (1989).

18 Enger R. C. and Case S. K., "Optical elements with ultrahigh spatial frequency surface corrugations," *Appl. Opt.* **22**, 3220 (1983), and references therein.

19 Dix C. and Mckee P. F., "High accuracy electron-beam grating lithography for optical and optoelectronic devices," *J. Vac. Sci. Technol.* **10**(6), 2667 (1992).

20 Swanton A., Armes D. J., Young-Smith K. J., Dix C., and Kashyap R., "Use of e-beam written, reactive ion etched, phase masks for the generation of novel photorefractive fibre gratings," *Special Issue, J. Micro. Electron. Eng.* **30**, 509–512 (1996).

21 Curran J. E., "Production of surface patterns by chemical plasma etching," *J. Phys. E.* **14**, 393–407 (1981).

22 Hill P. C. and Eggleton B. J., "Strain gradient chirp of fiber Bragg gratings," *Electron. Lett.* **30**, 1172–1174 (1994).

23 Kashyap R., McKee P. F., Campbell R. J., and Williams D. L., "A novel method of writing photo-induced chirped Bragg gratings in optical fibres," *Electron. Lett.* **12**, 996–997 (1994).

24 McKee P. F., Towers J. R., Wilkinson M. R., and Wood D., "New applications of optics from modern computer design methods," *BT Technol. J.* **11**(2), 161–169, (1993).

25 Pakulski G., Moore R., Maritan C., Shepard F., Fallahi M., Templeton I., and Champion G., "Fused silica masks for printing uniform and phase adjusted gratings for distributed feedback lasers," *Appl. Phys. Lett.* **62**(3), 222 (1993).

26 Kashyap R., Armitage J. R., Campbell R. J., Williams D. L., Maxwell G. D., Ainslie B. J., and Millar C. A., "Light-sensitive optical fibres and planar waveguides," *BT Technol. J.* **11**(2), 150–160 (1993).

27 Anderson D. Z., Mizrahi V., Erdogan T., and White A. E., "Phase-mask method for volume manufacturing of fiber phase gratings," Post-deadline paper PD16, *Technical Digest of Post-Deadline Papers Proc. Conf. on Optical Fiber Communications, OFC '93,* p. 68 (1993).

28 Hill K. O., Malo B., Bilodeau F., Johnson D. C., and Albert J., "Bragg grating fabricated in monomode photosensitive optical fiber by UV exposure through a phase mask," *Appl. Phys. Lett.* **62**(10), 1035 (1993).

29 Kashyap R., "Assessment of tuning the wave length of chirped and unchirped fibre Bragg grating with single phase masks," *Electron. Lett.*, **34**(21), 2025–2027 (1998).

30 Othonos A. and Lee X., "Novel and improved methods of writing Bragg gratings with phase masks," *IEEE Photon. Technol. Lett.* **7**(10), 1183–1185 (1995).

31 Dyer P. E., Farley R. J., Giedl R., Ragdale C., and Reid D., "Study and analysis of submicron-period grating formation on polymers ablated using a KrF irradiated phase mask," *Appl. Phys. Lett.* **64**(25), 3389–3391 (1995).

32 Parent M., Bures J., Lacroix S., and Lapierre J., "Propriétés de polarisation des réflecterus de Bragg induits par photosensibilité dans les fibres optiques monomode," *Appl. Opt.* **24**(3), 354 (1985).

33 Ouellette F., Gagnon D., and Porier M., "Permanent birefringence in Ge-doped fiber," *Appl. Phys. Lett.* **58**(17), 1813 (1991).

34 Bardal S., Kamal A., and Russell P. St. J., "Photoinduced birefringence in optical fibres: a comparative study of low-birefringence and high-birefringence fibers," *Opt. Lett.* **17**(6), 411 (1992).

35 An S. and Sipe J. E., "Polarisation aspects of two photon photosensitivity in birefringent optical fibres," *Opt. Lett.* **17**(7), 490 (1992).

36 Poirier M., Thibault S., Lauzon J., and Ouellette F., "Dynamic and orientational behaviour of UV induced luminescence bleaching in Ge-doped silica optical fiber," *Opt. Lett.* **18**(11), 870 (1993).

37 Wong D., Poole S. B., and Skeats M. G., "Stress-birefringence reduction in elliptical-core fibres under ultraviolet irradiation," *Opt. Lett.* **17**(24), 1773 (1992).

38 Vengsarkar A. M., Zhong Q., Inniss D., Reed W. A., Lemaire P. J., and Kosinski S. G., "Birefringence reduction in side written photoinduced fibre devices by a dual/circumferential exposure method," *Proc. Optical Fiber Conference, OFC'94,* post-deadline paper PD5, pp. 31–34 (1994).

39 Hill K. O., Bilodeau F., Malo B., and Johnson D. C., "Birefringent photosensitivity in monomode optical fibre: application to external writing of rocking filters," *Electron. Lett.* **27**(17), 1548 (1991).

40 Mizrahi V. and Sipe J. E., "Optical properties of photosensitive fiber phase gratings," *J. Lightwave Technol.* **1**, 1513–1517 (1993).

41 Kashyap R., Wyatt R., and McKee P. F., "Wavelength flattened saturated erbium amplifier using multiple side-tap Bragg gratings," *Electron. Lett.* **29**(11), 1025 (1993).

42 Martin J., Lauzon J., Thibault S., and Ouellette F., "Novel writing technique of long highly reflective in fiber gratings and investigation of the linearly chirped component," Post-deadline paper PD29-1, 138, *Proc. Conference on Optical Fiber Communications, OFC'94* (1994).

43 Byron K. C., Sugden K., Bircheno T., and Bennion I., "Fabrication of chirped Bragg gratings in photosensitive fibre," *Electron. Lett.* **29**(18), 1659 (1993).

44 Ouellette F., Eggleton B. J., Hill P. C., and Krug, P. A., "Chirp, self chirp and meta chirp in sampled Bragg gratings," in *Photosensitivity and Quadratic Nonlinearity in Glass Waveguides: Fundamentals and Applications,* Vol. 22, 1995 OSA Technical Series (Optical Society of America, Washington, DC, 1995), pp. PMC5, 247–250 (1995).

45 Ouellette F., Krug P., and Pasman R., "Characterization of long phase masks for writing fibre Bragg gratings," in *Photosensitivity and Quadratic Nonlinearity in Glass Waveguides: Fundamentals and Applications,* Vol. 22, 1995 OSA Technical Series (Optical Society of America, Washington, DC, 1995), pp. SuB7, 116–119 (1995).

46 Albert J., Theriault S., Bilodeau F., Johnson D. C., Hill K. O., Sixt P., and Rooks M. J., "Minimisation of phase errors in long fiber Bragg grating phase masks made using electron beam lithography," *IEEE Photon. Technol. Lett.* **8**(10), 1334–1336 (1996).

47 Kashyap R., Maxwell G. D., and Ainslie B. J., "Laser trimmed four-port bandpass filter fabricated in singlemode planar waveguides," *IEEE Photon. Technol. Lett.* **5**(2), 191 (1993).

48 Loh W. H., Cole M. J., Zervas M. N., and Laming R. I., "Compensation of imperfect mask with moving fibre-scanning beam technique for production of fibre gratings," *Electron. Lett.* **31**(17), 1483–1485 (1995).

49 Cole M. J., Loh W. H., Laming R. I., Zervas M. N., and Barcelos S., "Moving fibre/phase mask-scanning beam technique for enhanced flexibility in producing fibre gratings with a uniform phase mask," *Electron. Lett.* **31**(17), 92–94 (1995).

50 Eggleton B., Krug P. A., and Poladin L., "Dispersion compensation by using Bragg grating filters with self induced chirp," in *Tech. Digest Opt. Fib. Comm. Conf., OFC'94,* p. 227 (1994).

51 Kashyap R., Armitage J. R., Wyatt R. W., Davey S. T., and D. L., Williams, "All-fibre narrow-band reflection gratings at 150 nm," *Electron. Lett.* **26** (12), 730–731 (1990).

52 Chandra S., Takeuchi N., and Hartmann S. R., "Prism dye laser," *Appl. Phys. Lett.* **21**(4), 144–146 (1972).

53 Zhang Q., Brown D. A., Reinhart L., and Morse T. F., "Simple prism-based scheme for fabricating Bragg gratings in optical fibres," *Opt. Lett.* **19**(23), 2030–2032 (1994).

54 Rizvi N. H. and Gower M. C., "Production of submicron period Bragg gratings in optical fibers using wavefront division with a biprism and an excimer laser source," *Appl. Phys. Lett.* **67**(6), 739–741, (1995).

55 Rizvi N. H., Gower M. C., Godall F. C., Arthur G., and Herman P., "Excimer laser writing of submicrometre period fiber Bragg gratings using a phase-shifting mask projection," *Electron. Lett.* **31**(11), 901–902 (1995).

56 Mihailov S. J. and Gower M. C., "Recording of efficient high-order Bragg reflectors in optical fibres by mask image projection and single pulse exposure with an excimer laser," *Electron. Lett.* **30**(9), 707–709 (1994).

57 Malo B., Bilodeau F., Albert J., Johnson D. C., Hill K. O., Hibino Y., and Abe M., "Photosensitivity in optical fiber and silica on substrate waveguides," *SPIE* **2044**, 46–54 (1993).

58 Kanellopoulos S. E., Valente L. C. G., Handerek V. A., and Rogers A. J., "Comparison of photorefractive effects and photogenerated components in polarisation maintaining fibres," *SPIE* **1516**, "International Workshop of Photoinduced Self-Organisation effects in Optical Fibres," p. 200 (1991), and references therein.

59 Stolen R. H., Ashkin A., Pliebel W., and Dziedzic J. M., "In-line fiber-polarisation-rocking rotator and filter," *Opt. Lett.* **9**, 300–303 (1984).

60 Russell P. St. J. and Hand D. P., "Rocking filter formation in photosensitive high birefringence optical fibres," *Electron. Lett.* **26**, 1846–1848 (1990).

61 Johnson D. C., Bilodeau F., Malo B., Hill K. O., Wigley P. G. J., and Stegeman G. I., "Long length, long-period rocking filters fabricated from conventional monomode telecommunications optical fibers," *Opt. Lett.* **17**(22), 1635 (1992).

62 Park H. G. and Kim B. Y., "Intermodal coupler using permanently photoinduced grating in two mode optical fibre," *Electron. Lett.* **25**(12), 797 (1989).

63 Hill K. O., Malo B., Vineberg K. A., Bilodeau F., Johnson D. C., and Skinner I., "Efficient mode conversion in telecommunication fiber using externally written gratings," *Electron. Lett.* **26**, 1270–1272 (1990).

64 Bilodeau F., Hill K. O., Malo B., Johnson D. C., and Skinner I. M., "Efficient, narrowband $LP_{01} \leftrightarrow LP_{02}$ mode converters fabricated in photosensitive fiber: Spectral response," *Electron. Lett.* **27**, 682–682, (1991).

65 Ulrich R., Rashleigh S. C., and Eichoff W., "Bending induced birefringence in single mode fibres," *Opt. Lett.* **5**, 273–275 (1980).

66 Lefevre H. C., "Single-mode fibre fractional wave devices and polarisation controllers," *Electron. Lett.* **16**, 778–779 (1980).

67 Dyott R. B., Cozens J. R., and Morris D. G., "Preservation of polarisation in optical-fibres with elliptical cores," *Electron. Lett.* **19**, 380–382 (1979).

68 Morey W. W., Meltz G., Love J. D., and Hewlett S. J., "Mode-coupling characteristics of photo-induced Bragg gratings in depressed cladding fiber," *Electron. Lett.* **30**, 730–731 (1994).

69 Ouellette F., "Phase-matching of optical fibre photosensitive intermodal couplers in infra-red," *Electron. Lett.* **25**(23), 1590–1591 (1989).

70 Espinola R. P., Atkins R. M., Wang N. P., Simoff D. A., Paczkowski M. A., Windeler R. S., Brownlow D. L., Shenk D. S., Glodis P. A., Strasser T. A., DeMarco J. J., and Chandonnet P. J., "40 dB fiber Bragg grating written through the fiber coating at 257 nm," in *Bragg Gratings, Photosensitivity, and Poling in Glass Fibers and Waveguides: Applications and Fundamentals,* Vol. 17, OSA Technical Digest Series (Optical Society of America, Washington, DC, 1997), post-deadline paper PD2.

71 Starodubov D. S., Grubsky V., Feinberg J., Disnov D., Semjonov S. L., Guryanov A. N., and Vechkanov N. N., "Fiber Bragg gratings with reflectivity >97% fabricated through polymer jacket using near-UV radiation," in *Bragg Gratings, Photosensitivity, and Poling in Glass Fibers and Waveguides: Applications and Fundamentals,* Vol. 17, OSA Technical Digest Series (Optical Society of America, Washington, DC, 1997), post-deadline paper PD1.

72 Vengsarkar A. M., Lemaire P. J., Judkins J. B., Bhatia V., Erdogan T., and Sipe J. E., "Long period fiber gratings as band rejection filters," *IEEE J. Lightwave. Technol.* **14**, 58–64 (1996).

73 Stubbe R., Sahlgren B., Sandgren S., and Asseh A., "Novel technique for writing long superstructured fiber Bragg gratings," in *Photosensitivity and Quadratic Nonlinearity in Glass Waveguides: Fundamentals and Applications,* Vol. 22, 1995 OSA Technical Series (Optical Society of America, Washington, DC, 1995), pp. PD1-(1–3) (1995).

74 Kashyap R., Froehlich H-G., Swanton A., and Armes D. J., "Super-step-chirped fibre Bragg gratings," *Electron. Lett.* **32**(15), 1394–1396 (1996).

75 Kashyap R., Froehlich H-G., Swanton A., and Armes D. J., "1.3 m long super-step-chirped fibre Bragg grating with a continuous delay of 13.5 ns and bandwidth 10 nm for broadband dispersion compensation," *Electron. Lett.* **32**(19), 1807–1809 (1996).

76 Zhang Q., Brown D. A., Reinhart L., Morse T. F., Wang J. Q., and Xiao G., "Tuning Bragg wavelength by writing gratings on prestrained fibers," *IEEE Photon. Technol. Lett.* **6**(7), 839–841 (1994).

77 Legoubin S., Fertein E., Douay M., Bernage P., Niay P., Bayon F., and Georges T., "Formation of Moiré gratings in core of germanosilicate fibre by transverse holographic double exposure," *Electron. Lett.* **27**(21), 1945 (1991).

78 Sugden K., Zhang L., Williams J. A. R., Fallon L. A., Everall L. A., Chisholm K. E., and Bennion I., "Fabrication and characterization of bandpass filters based on concatenated chirped fiber gratings," *IEEE J. Lightwave Technol.* **15**(8), 1424–1432 (1997).

79 Byron K. C., Sugden K., Bircheno T., and Bennion I., "Fabrication of chirped Bragg gratings in photosensitive fibre," *Electron. Lett.* **29**(18), 1659 (1993).

80 Putnam M. A., Williams G. M., and Friebele E. J., "Fabrication of tapered, strain-gradient chirped fibre Bragg gratings," *Electron. Lett.* **31**(4), 309–310 (1995).

81 Martin J., Lauzon J., Thibault S., and Ouellette F., "Novel writing technique of long highly reflective in fiber gratings and investigation of the linearly chirped component," post-deadline paper PD29-1, 138, *Proc. Conference on Optical Fiber Communications, OFC'94* (1994).

82 Morey W. W., Meltz G., and Glenn W. H.,"Fiber optic Bragg grating sensors," *SPIE* **1169**, *Fibre Optics Sensors VII*, pp. 98–107 (1989).

83 Kringlebotn J. T., Morkel P. R., Reekie L., Archambault J. L., and Payne D. N., "Efficient diode-pumped single frequency erbium:ytterbium fibre laser," *IEEE Photon. Technol. Lett.* **5**(10), 1162 (1993).

84 Canning J. and Skeats M. G., "π-Phase shifted periodic distributed structures in optical fibers by UV post-processing," *Electron. Lett.* **30**(16), 1244–1245 (1994).

85 Agrawal G. P. and Radic S., "Phase-shifted fiber Bragg gratings and their applications for wavelength demultiplexing," *IEEE Photon. Technol. Lett.* **6**, 995–997 (1994).

86 Jayaraman V., Cohen D. A., and Coldren L. A., "Demonstration of broadband tunability of a semiconductor laser using sampled gratings," *Appl. Phys. Lett.* **60**(19), 2321–2323 (1992).

87 Eggleton B. J., Krug P. A., Poladin L., and Ouellette F., "Long periodic superstructure Bragg gratings in optical fibres," *Electron. Lett.* **30**(19), 1620–1621 (1994).

88 Ouellette F., Krug P. A., and Pasman R., "Characterisation of long phase masks for writing fibre Bragg gratings," in *Photosensitivity and Quadratic Nonlinearity in Glass Waveguides: Fundamentals and Applications*, Vol. 22, 1995 OSA Technical Series (Optical Society of America, Washington, DC, 1995), pp. 116–119.

89 Legoubin S., Douay M., Bernage P., Niay, Boj S., and Delevaque E., "Free spectral range variations of grating-based Fabry–Perot photowritten in optical fibers," *J. Opt. Soc. Am. A* **12**(8), 1687–1694 (1995).

90 Zengerle R. and Leminger O., "Phase-shifted Bragg-grating filters with improved transmission characteristics," *J. Lightwave Technol.* **13**, 2354–2358 (1995).

91 Storøy H., Engan H. E., Sahlgren B., and Stubbe R., "Position weighting of fibre Bragg gratings for bandpass filtering," *Opt. Lett.* **22**(11), 784–786 (1997).

92 Kashyap R, McKee P. F., and Armes D., "UV written reflection grating structures in photosensitive optical fibres using phase-shifted phase-masks," *Electron. Lett.* **30**(23), 1977–1979 (1994).

93 Ibsen M., Eggleton B. J., Sceats M. G., and Ouellette F., "Broadly tunable DBR fibre using sampled Bragg gratings," *Electron. Lett.* **31**(1), 37–38, (1995).

94 Byron K. C., Sugden K., Bircheno T., and Bennion I., "Fabrication of chirped Bragg gratings in a photo sensitive fibre," *Electron. Lett.* **29**(18), 1659–1660 (1993).

95 Krug P. A., Stephens T., Yoffe G., Ouellette F., Hill P., and Doshi G., "270 km transmission at 10Gb/s in nondispersion shifted fiber using an adjustably chirped 120 mm long fiber Bragg grating dispersion compensator," in *Tech. Digest Conf. on Opt. Fiber Commun., OFC'95,* post-deadline paper PDP27 (1995).

96 Kashyap R., McKee P. F., Campbell R. J., and Williams D. L., "A novel method of writing photo-induced chirped Bragg gratings in optical fibres," *Electron. Lett.* **12**, 996–998 (1994).

97 Delavaque E., Boj S., Bayon J-F., Poignant H., Le Mellot J., Monerie M., Niay P., and Bernage P., "Optical fiber design for strong grating photo imprinting with radiation mode suppression," in *Proc. Post-Deadline Papers of OFC'95,* paper PD5 (1995).

98 Sugden K., Bennion I., Moloney A., and Cooper N. J., "Chirped grating produced in photosensitive optical fibres by fibre deformation during exposure," *Electron. Lett.* **30**(5), 440–441 (1994).

99 Dong L., Cruz J. L., Reekie L., and Trucknott J. A., "Fabrication of chirped fibre gratings using etched tapers," *Electron. Lett.* **31**(11), 908–909 (1995).

100 Dong L., Cruz J. L., Reekie L., and Trucknott J. A., "Chirped fiber Bragg gratings fabricated using etched tapers," *Opt. Fiber Technol.* **1**, 363–368 (1995).

101 Okude S., Sakai T., Wada A., and Yamauchi R., "Novel chirped fiber grating utilizing a thermally diffused taper-core fiber," in *Proc. OFC'96,* paper TuO7, pp. 68–69 (1996).

102 Shiraishi K., Aizawa Y., and Kawakami S., *J. Lightwave Technol.* **8**, 1151 (1990).

103 Byron K. C. and Rourke H. N., "Fabrication of chirped fibre gratings by novel stretch and write technique," *Electron. Lett.* **31**(1), 60–61 (1995).

104 Farries M. C., Sugden K, Reid D. C. J., Bennion I., Molony A., and Goodwin M. J., "Very broad reflection bandwidth (44 nm) chirped fibre gratings and narrow-bandpass filters produced by the use of an amplitude mask," *Electron. Lett.* **30**(11), 891–892 (1994).

105 Kashyap R., "Design of step-chirped fibre Bragg gratings," *Opt. Comm.*, **136**(5–6), 461–469 (1997).

106 Kashyap R., Chernikov S. V., Mckee P. F., and Taylor J. R., "30 ps chromatic dispersion compensation of 400 fs pulses at 100 Gbits/s in optical fibres using an all fibre photoinduced chirped reflection grating," *Electron. Lett.* **30**(13), 1078–1079 (1994).

107 Kawase L. R., Carvalho M. C. R., Margulis W., and Kashyap R., "Transmission of chirped optical pulses in fibre-grating dispersion compensated system," *Electron. Lett.* **33**(2), pp. 52–54 (1997).

108 Kashyap R., Swanton A., and Armes D. J., "A simple technique for apodising chirped and unchirped fibre Bragg gratings," *Electron. Lett.* **32**(14), 1227–1228 (1996).

109 Riant I. and Sansonetti P., "New method to control chirp and wavelength of fibre Bragg gratings for multichannel chromatic dispersion compensation", in Colloquium on Optical Fibre Gratings, *IEE Ref.*, 1997/037, pp. 18/1-18/3, London (1997).

110 Kashyap R., Maxwell G. D., and Ainslie B. J., "Laser-trimmed four-port bandpass filter fabricated in single-mode photosensitive Ge-doped planar waveguide," *IEEE J. Photon. Technol.* **5**(2), 191–194 (1993).

111 Kashyap R., unpublished.

112 Kashyap R., Ellis A., Malyon D., Froehlich H-G., Swanton A., and Armes D. J., "Eight wavelength × 10Gb/s simultaneous dispersion compensation over 100km singlemode fibre using a single 10 nm bandwidth, 1.3 metre long, super-step-chirped fibre Bragg grating a continuous delay of 13.5 ns," in *Proc. Post-Deadline Papers of the 22nd ECOC'97,* Oslo, Norway, Sept. 15–19, 1996.

113 Archambault J-L., Ph.D. Thesis, Southampton University, United Kingdom (1994).

114 Xie W. X., Niay P., Bernage P., Douay M., Bayon J. F., Georges T., Monerie M., and Poumellec B., "Experimental evidence of two types of photorefractive

effects occurring during photoinscription of Bragg gratings within germanosilicate fibers," *Opt. Commun.* **104**, 185–195 (1993).

115 Duval Y., Kashyap R., Fleming S., and Ouellette F., "Correlation between ultraviolet-induced refractive index change and photoluminescence in Ge-doped fibre," *Appl. Phys. Lett.* **61**(25) 2955 (1992).

116 Limberger H. G., Limberger P. Y., and Salathé R., "Spectral characterization of photoinduced high efficient Bragg gratings in standard telecommunication fibers," *Electron. Lett.*, **29**(1), 47–49 (1993).

117 Kashyap R. and Maxwell G. D., unpublished (1991).

118 Askins C. G., Tsai T-E., Williams G. M., Puttnam M. A., Bashkansky M., and Friebele E. J., "Fibre Bragg reflectors prepared by a single excimer pulse," *Opt. Lett.* **17**(11), 833 (1992).

119 Archambault J-L., Reekie L., and Russell P. St. J., "High reflectivity and narrow bandwidth fibre gratings written by a single excimer pulse," *Electron. Lett.* **29**(1), 28 (1993).

120 Malo B., Johnson D. C., Bilodeau F., Albert J., and Hill K. O., "Single-excimer-pulse writing of fiber gratings by use of a zero-order nulled phase mask: grating spectral response and visualization of index perturbations," *Opt. Lett.* **18**(15), 1277 (1993).

121 Archambault J-L., Reekie L., and Russell P. St. J., "100% reflectivity Bragg reflectors produced in optical fibres by single excimer pulses," *Electron. Lett.* **29**(5), 453 (1993).

122 Askins C. G., Putnam M. A., Williams G. M., and Friebele E. J., "Stepped-wavelength optical-fiber Bragg grating arrays fabricated in line on a draw tower," *Opt. Lett.* **19**(2), 147–149 (1994).

123 Dong L., Archambault J. L., Reekie L., Russell P. St. J., and Payne D. N., "Single pulse Bragg gratings written during fibre drawing," *Electron. Lett.* **29**(17), 1577 (1993).

124 Mizrahi V. and Sipe J. E., "Optical properties of photosensitive fiber phase gratings," *Lightwave Technol.* **11**(10), 1513–1517 (1993).

125 Dong L., Archambault J. L., Reekie L., Russell P. St. J., and Payne D. N., "Single pulse Bragg gratings written during fibre drawing," *Electron. Lett.* **29**(17), 1577 (1993).

126 Patrick H., and Gilbert S. L., "Growth of Bragg gratings produced by continuous-wave ultra-violet light in optical fiber," *Opt. Lett.* **18**(18), 1484 (1993).

127 Armitage J. R., "Fibre Bragg reflectors written at 262 nm using frequency quadrupled Nd^{3+}:YLF," *Electron. Lett.* **29**(13), 1181–1183 (1993).

128 Dianov E. M., and Starodubov D. S., "Microscopic mechanisms of photosensitivity in germanium-doped silica glass," *SPIE Proc, 2777,* pp. 60–70 (1995).

129 Starodubov D. S., Dianov E. M., Vasiliev S. A., Frolov A. A., Medvedkov O. I., Rybaltovskii A. O., and Titova V. A., "Hydrogen enhancement of near-UV photosensitivity of germanosilicate glass," *SPIE Proc. 2998,* pp. 111–121 (1997).

130 Starodubov D. S., Grubsky V., Feinberg J., and Erdogan T., "Near-UV fabrication of ultrastrong Bragg gratings in hydrogen loaded germanosilicate fibers," *Proc. of CLEO'97,* post-deadline paper CDP24, 1997.

131 Patrick H. J., Askins C. G., McElhanon R. W. and Friebele E. J. *Electron. Lett., 33*(13), 1167–1168, 19 June 1997.